

AEROSPACE INFORMATION REPORT

AIR6504™

Issued Reaffirmed 2017-10 2022-06

Procedure for the Calculation of Non-Volatile Particulate Matter Sampling and Measurement System Penetration Functions and System Loss Correction Factors

RATIONALE

This SAE Aerospace Information Report (AIR) describes a method for calculating correction factors to account for system particle losses when performing non-volatile Particulate Matter (nvPM) measurement as specified in AIR6037. Such sampling and measurement systems have significant line length and several components that result in particle losses. The particle losses are size dependent and hence depend on many factors including combustor technology and engine operating condition resulting in a reduction in measurement of the order of 50% for nvPM mass concentration and 90% for nvPM number concentration. Estimation of engine exit plane nvPM mass and number concentrations are improved by developing a calculation method to account for these losses.

The approach used in this AIR will involve separate correction factors for measured not mass and number concentrations, which will be calculated using measured or calculated line and component penetration efficiencies. These calculations will be based on assumptions of a lognormal particle size distribution at the engine exit with a known associated lognormal width, and an equivalent spherical particle shape with a corresponding known effective particle density. These resulting correction factors will then be used to estimate the total particle losses in the sampling and measurement system for nvPM mass and number, and will thus be used to infer the engine exit plane concentrations of nvPM mass and number.

SAENORM. COM. Click to VI AIR6504 has been reaffirmed to comply with the SAE Five-Year Review policy.

SAE Executive Standards Committee Rules provide that: "This report is published by SAE to advance the state of technical and engineering sciences. The use of this report is entirely voluntary, and its applicability and suitability for any particular use, including any patent infringement arising therefrom, is the sole responsibility of the user."

SAE reviews each technical report at least every five years at which time it may be revised, reaffirmed, stabilized, or cancelled. SAE invites your written comments and suggestions.

Copyright © 2022 SAE International

All rights reserved. No part of this publication may be reproduced, stored in a retrieval system or transmitted, in any form or by any means, electronic, mechanical, photocopying, recording, or otherwise, without the prior written permission of SAE.

TO PLACE A DOCUMENT ORDER: 877-606-7323 (inside USA and Canada) Tel:

Tel: +1 724-776-4970 (outside USA) Fax: 724-776-0790

Email: CustomerService@sae.org

http://www.sae.org

For more information on this standard, visit https://www.sae.org/standards/content/AIR6504/

SAE WEB ADDRESS:

TABLE OF CONTENTS

1.	SCOPE	3
1.1	Sections	3
_		
2.	REFERENCES, DEFINITIONS, TERMINOLOGY, AND UNITS	4
2.1	Applicable Documents	
2.2	Definitions	
2.3	Symbols, Acronyms, and Terminology	
2.4	Units	13
	INTRODUCTION	4.4
3.	INTRODUCTION	
3.1	Background	14
3.2	Overview of the Procedure to Assess System Loss, Calculate System Penetration Functions,	4-
	and Estimate Correction Factors	
3.3	Note on Particle Diameters	15
3.4	Particle Size Distribution	16
3.5	Correction Method Overview	17
1 .	SYSTEM PENETRATION CALCULATIONS	10
+. 4.1	Required Parameters to Determine System Losses	10
+. 1 4.2	Measured nvPM Mass and Number	19
4.3	United Technologies Research Center (UTRC) Line Penetration Function Calculation Method	
1.4	Note on Penetration Measurements	22
4.5	Calculation of Penetration Functions	
4.6	Diffusional, Thermophoretic, and Bend Penetration Fractions from the UTRC Model	
4.7	Penetration Fractions Due to Inertial Particle Losses in Bends from the UTRC Model, η _{bi} (D _m)	
4.8	Thermophoresis	26
4.9	Diluter1 Penetration Fraction	27
4.10	Splitter Penetration Fractions	27
4.11	Cyclone Separator and VPR Penetration Functions and CPC Counting Efficiencies	27
_	SIZE DISTRIBUTIONS AND SYSTEM LOSS CORRECTION FACTOR ESTIMATION	20
5. -	SIZE DISTRIBUTIONS AND SYSTEM LOSS CORRECTION FACTOR ESTIMATION	30
5.1	Size Distribution Assumptions	30
5.2	Methodology for Estimating Engine Exhaust Plane Size Distributions	31
5.3	nvPM Mass and Number Correction Factors	33
6.	UNCERTAINTIES IN NORM MASS AND NUMBER CORRECTION FACTORS	3/
5. 5.1	Parameter Uncertainties	
5.2	Overview of Monte Carlo Method	
5.3	Results	36
7	GENERAL NFORMATION ON METHOD ASSUMPTIONS AND ASSESSMENTS	30
7.1	Assumptions	
7.2	Collection Part Penetration Function, η ₁ (D _m)x η _{b1} (D _m)	33
7.3	Assessments	
	Assessifients	42
3.	EXAMPLES OF SYSTEM LOSS CORRECTION METHODOLOGY	45
3.1	Example 1, Cyclone Separator Penetration Function	
3.2	Example 2, VPR Penetration Function	
3.3	Example 3, CPC Counting Efficiency Function	
3.4	Example 4, Example of Mass at LOD Calculation	
J. -T	Example 4, Example of Iviass at LOD Galculation	31
9.	NOTES	54
9.1	Revision Indicator	
APPENDIX A	PENETRATION FUNCTION DETAILS	
APPENDIX B	DETERMINATION OF CORRECTION FACTORS	
APPENDIX C	ERROR DETERMINATION DETAILS	64

1. SCOPE

This SAE Aerospace Information Report (AIR) describes a method for assessing size dependent particle losses in a sampling and measurement system of specified geometry utilizing the non-volatile PM (nvPM) mass and number concentrations measured at the end of the sampling system. The penetration functions of the sampling and measurement system may be determined either by measurement or by analytic computational methods.

Loss mechanisms including thermophoretic (which has a very weak size dependence) and size dependent losses are considered in this method² along with the uncertainties due to both measurement error and the assumptions of the method. The results of this system loss assessment allow development of estimated correction factors for nvPM mass and number concentrations to account for the system losses facilitating estimation of the nvPM mass and number at the engine exhaust nozzle exit plane. As the particle losses are size dependent, the magnitude of correction factors can vary as a function of many factors including combustor technology and engine operating condition.

Implementation of the nvPM sampling and measurement system for aircraft engine testing, as per AIR6037, requires a sample line of up to 35 m and includes several sampling and measurement system components, which result in significant particle loss on the order of 50% for nvPM mass and 90% for nvPM number.

The system loss correction factors are estimated based on a model with the following inputs and assumptions: engine exhaust exit plane nvPM have a lognormal distribution, known size dependent values of nvPM effective density and geometric standard deviation, a minimum particle size cut-off of 10 nm, and no coagulation.

1.1 Sections

This document is divided into the following sections and appendices:

- 2. Reference, Definitions, Terminology, and Units
- 3. Introduction
- 4. System Penetration Calculations
- Size Distributions and System Loss Correction Factor Estimation
- 6. Uncertainties in nvPM Mass and Number Correction Factors
- 7. General Information on Method Assumptions and Assessments
- 8. Examples of System Loss Correction Methodology
- 9. Notes

The solution method presented here is fully equivalent to that published in ICAO Annex 16 Vol. II Amendment 9. The underlying mathematics and inputs are identical and the method has been verified that it produces identical outputs. The computational methodology has been modified to make the numerical calculations more efficient and reduce computational uncertainties.

The predominate system loss mechanisms that influence the measured values of mass and number are diffusional, thermophoretic, and losses in bends. These three loss mechanisms are the mechanisms taken into consideration in this method. The system loss mechanisms in the attached loss calculation tools include additional loss mechanisms (electrostatic and turbulent inertial losses in lines) but the functionality has been disabled. The research loss calculation tools include the functionality for these additional loss mechanisms. The user manuals for the tools discuss this in more detail.

APPENDICES:

- A: Penetration Function Details
- B: Determination of Correction Factors
- C: Error Determination Details

ATTACHMENTS:

- I: Expert Review (Prof. David Kittelson) (Attachment I Review DBK.pdf)
- II: Expert Review (Prof. Max Zhang) (Attachment II Review KMZ.pdf)
- III: Excel® spreadsheet line loss tool (nvPM Line Loss Tool v1_0_Release.xlsm)
- IV: Excel® spreadsheet users guide (Excel Users_Guide_App7LineLossTool_v1_0 Release.pdf)
- V: Excel® spreadsheet setup guide (Excel nvPMLineLossToolSetup v1_0 Release.pdf)
- VI: Excel® spreadsheet with standard input data set (STDdataset28Jun2016.xlsx)
- VII: MATLAB® line loss tool installer (Matlab LineLossCalc_v1_0 Release.mlappinstall)
- VIII: MATLAB® users guide (MatlabLineLossCalc UserGuide v1_0 Release.pdf)
- 2. REFERENCES, DEFINITIONS, TERMINOLOGY, AND UNITS

The following publications form a part of this document to the extent specified herein. The latest issue of SAE publications shall apply. The applicable issue of other publications shall be the issue in effect on the date of the purchase order. In the event of conflict between the text of this document and references cited herein, the text of this document takes precedence. Nothing in this document, however, supersedes applicable laws and regulations unless a specific exemption has been obtained.

- 2.1 Applicable Documents
- 2.1.1 SAE Publications

Available from SAE International, 400 Commonwealth Drive, Warrendale, PA 15096-0001, Tel: 877-606-7323 (inside USA and Canada) or +1 724-776-4970 (outside USA), www.sae.org.

- 2.1.1.1 AIR6241, Procedure for the Continuous Sampling and Measurement of Non-Volatile Particle Emissions from Aircraft Turbine Engines
- 2.1.1.2 AIR6037, Aircraft Exhaust Nonvolatile Particle Matter Measurement Method Development
- 2.1.1.3 Kittelson, D. and Johnson, J., "Variability in Particle Emission Measurements in the Heavy Duty Transient Test," SAE Technical Paper 910738, 1991, doi:10.4271/910738.
- 2.1.1.4 AIR5892, Nonvolatile Exhaust Particle Measurement Techniques
- 2.1.1.5 ARP1179, Aircraft Gas Turbine Engine Exhaust Smoke Measurement
- 2.1.2 Appended Documents

See attachments.

- 2.1.3 Other publications
- 2.1.3.1 P.Lobo, D.E.Hagen, P.D.Whitefield, D.J.Alofs, Physical Characterization of Aerosol Emissions from a Commercial Gas Turbine Engine, Journal of Propulsion and Power, Vol. 23, No. 5, September–October 2007.

- 2.1.3.2 R.P.Howard, K.M.Stephens, P.D.Whitefield, D.E.Hagen, S.L.Achterberg, E.A.Black, S.C.Herndon, M.T.Timko, R.C.Miake-Lye, J.S.Kinsey, and D.Gemmill, Interim Particulate Matter Test Method For The Determination Of Particulate Matter From Gas Turbine Engines, SERDP Project WP-1538, Final Report, 29-July 2011.
- 2.1.3.3 A.Crayford, M.Johnson, R.Marsh, Y.Sevcenco, D.Walters, P.Williams, S.Christie, W.Chung, A.Petzold, A.Ibrahim, D.Delhaye, P.Quincey, P.Bowen, H.Coe, D.Raper, C.Wilson, SAMPLE III-SC01: Studying, sampling and measuring of aircraft particulate emissions, Final Report, 23rd October 2011 (http://easa.europa.eu/document-library/research-projects/easa2010fc10-sc01).
- 2.1.3.4 A.Crayford, M.Johnson, R.Marsh, Y.Sevcenco, D.Walters, P.Williams, A.Petzold, P.Bowen, J.Wang, D.Lister, SAMPLE III-SC02: Studying, sampling and measuring of aircraft particulate emissions, Final Report, 27th November 2012 (http://easa.europa.eu/document-library/research-projects/easa2010fc10-sc02).
- 2.1.3.5 A.Crayford, M.Johnson, A.Llamedo, P.Williams, P.Madden, R.Marsh, P.Bowen, SAMPLE III-SC03: Studying, sampling and measuring of aircraft particulate emissions, Final Report, 15th November 2013 (http://easa.europa.eu/document-library/research-projects/easa2010fc10-sc03).
- 2.1.3.6 A.Crayford, M.Johnson, Y.Sevcenco, P.Williams, SAMPLE III-SC05: Studying, sampling and measuring of aircraft particulate emissions, Final Report, 15 November 2014 http://easa.europa.eu/document-library/research-projects/easa2010fc10-sc05).
- 2.1.3.7 L.Durdina, B.T.Brem, M.Abegglen, P.Lobo, T.Rindlisbacher, K.A.Thomson, G.J.Smallwood, D.E.Hagen, B.Sierau, J.Wang, Determination of PM mass emissions from an aircraft turbine engine using particle effective density, Atmospheric Environment, vol. 99, pp.500-507 (2014).
- 2.1.3.8 J.Kinsey, Characterization of Emissions from Commercial Arcraft Engines during the Aircraft Particle Emissions eXperiment (APEX) 1 to 3. U.S. EPA Report EPA-600/R_c09/130, October 2009.
- 2.1.3.9 B.E.Anderson, A.J.Beyersdorf, C.H.Hudgins, J.V.Plant, K.L.Thornhill, E.L.Winstead, L.D.Ziemba, R.Howard, E.Corporan, R.C.Miake-Lye, S.C.Herndon, M.Timko, E.Woods, W. Dodds, B.Lee, G.Santoni, P.Whitefield, D.Hagen, P.Lobo, W.B.Knighton, D.Bulzan, K.Tacina, C. Wey, R.Vander Wal, A.Bhargava, J.Kinsey, D.S.Liscinsky, Alternative Aviation Fuel Experiment (AAFEX), NASA Report NASA/TM–2011-217059, February 2011.
- 2.1.3.10 P.Lobo, L.Durdina, G.Smallwood, T.Rindlisbacher, F.Siegerist, E.Black, Z.Yu, A.Mensah, D.Hagen, R.Miake-Lye, K.Thomson, B.Brem, J.Corbin, M.Abegglen, B.Sierau, P.Whitefield, J.Wang, Measurement of Aircraft Engine Non-Volatile PM Emissions, Results of the Aviation-Particle Regulatory Instrumentation Demonstration Experiment (A-PRIDE) 4 Campaign, Aerosol Sci. & Techn. Vol. 49, #7, 472-484 (2015)
- 2.1.3.11 D.Kittelson, E31 committee communications, DP19_Toulouse_18-21Jul2016_VARIAnT Report_DKittelson and DP03_Tullahoma_Mar2016_ Variant 2 line loss measurements_DKittelson
- 2.1.3.12 Liscinsky, D.S. and Hollick, H.H., Effect of Particle Sampling Technique and Transport on Particle Penetration at the High Temperature and Pressure Conditions found in Gas Turbine Combustors and Engines, NASA/CR-2010-NNC07CB03C, Mar 2010.
- 2.1.3.13 A.Bhargava, D.Liscinsky, R.McKinney, B.Anderson, A.Petzold, R.C.Miake-Lye, Characterizing Particulate Matter Emissions from Aircraft Engines, ASME Turbo Expo, paper no. GT2012-69598 (2012).
- 2.1.3.14 S.J.Yook and D.Y.H.Pui, Estimation of Penetration Efficiencies through NASA Sampling Lines, submitted to NASA Glenn Research Center (2005).
- 2.1.3.15 P.A.Baron and K.Willeke, Aerosol measurement: Principles, Techniques, and Applications, Wiley (2001).

- 2.1.3.16 P.A.Baron, Description of an aerosol calculator, Proceedings of the Seventh International Aerosol Conference, eds. P.Biswas, D.R.Chen, and S.Herings, September 10-15, 2006, St. Paul, Minnesota, e.g., http://aerosols.wustl.edu/AAARworkshop08/html/calculator.htm (last accessed January 2016) and http://www.cdc.gov/niosh/nioshtic-2/20044864.html (last accessed January 2016).
- 2.1.3.17 W.Birmili, K.Stopfkuchen, M.Hermann, A.Wiedensohler, and J.Heintzenberg, Particle Penetration Through a 300 m Inlet Pipe for Sampling Atmospheric Aerosols from a Tall Meteorological Tower, Aerosol Science and Technology, volume 41, pp. 811–817 (2007).
- 2.1.3.18 D.B.Kittelson, Expert Review of SAE E-31 Method to Estimate Emissions of Non-Volatile Particulate Matter (nvPM) from Aircraft Engines and Correct for Sample Train Losses, (unpublished report to U.S. EPA, contract EP-C-12-011, work assignment 2-22), August 8, 2013.
- 2.1.3.19 P.G.Gormley, and M.Kennedy, Diffusion from a stream flowing through a cylindrical tube, Proceedings of the Royal Irish Academy, vol 52A, pp163-169 (1949).
- 2.1.3.20 N.A.Fuchs, The Mechanics of Aerosols, Dover (1989).
- 2.1.3.21 W.C.Hinds, Aerosol Technology: Properties, Behavior, and Measurement of Airborne Particles, John Wiley and Sons (1982).
- 2.1.3.22 K.Willeke, Temperature Dependence of Particle Slip in a Gaseous Medium, Journal of Aerosol Science, volume 7, pp. 381 to 387 (1976).
- 2.1.3.23 M.D.Allen and O.G.Raabe, Re-Evaluation of Millikan's Oil Drop Data for the Motion of Small Particles in Air, Journal of Aerosol Science, volume 13, number 6, pp. 537-547(1982).
- 2.1.3.24 S.K.Friedlander, Smoke, Dust, and Haze Fundamentals of Aerosol Dynamics, Oxford University Press (2000).
- 2.1.3.25 L.Waldmann and K.H.Schmitt, Thermophoresis and Diffusiophoresis of Aerosols, in Aerosol Science, C.N.Davies (ed.), Academic Press (1966).
- 2.1.3.26 B.Giechaskiel, L.Ntziachristos, and Z.Samaras, Effect of ejector dilutors on measurements of automotive exhaust gas aerosol size distributions, Meas. Sci. Technol., vol 20, 045703, (2009).
- 2.1.3.27 T.M.Peters and R.W.Vanderpoot, Modification and Evaluation of the WINS Impactor R.T.I. Report No. 6360-011 (1996).
- 2.1.3.28 M.E.Moore and A.R.McFarland, Design Methodology for Multiple Inlet Cyclones, Environ. Sci. Technology, vol. 30, pp 271-276 (1996)
- 2.1.3.29 L.C.Kenny and R.A.Gussman, Characterization and Modelling of a Family of Cyclone Aerosol Preseparators, Journal of Aerosol Science, vol 28, #4, pp 677-688 (1997).
- 2.1.3.30 L.C.Kenny, R.Gussman, and M.Meyer, Development of a Sharp-Cut Cyclone for Ambient Aerosol Monitoring Applications, Aerosol Science and Technology,32:4, 338-358 (2000).
- 2.1.3.31 M.R.Stolzenburg and P.H.McMurry, An Ultrafine Aerosol Condensation Nucleus Counter, Aerosol Science and Technology, 14:1, 48-65 (1991).
- 2.1.3.32 D.Hagen, E31 committee communication, DP28_Boston_2-6Jun2014_MST and EMPA Sampling Systems Assessment of Penetration DHagen
- 2.1.3.33 D.Liscinsky, E31 committee communication, DP43 Boston 2-6Jun2014 LineLossTeam FrontEnd DLiscinsky
- 2.1.3.34 K.M.Zhang, Review Comments on the Proposed Method for Analyzing and Correcting Mass and Number Measurements for Line Losses, (unpublished report to U.S. EPA, contract EP-C-12-011, work assignment 2-22), June 2013.

- 2.1.3.35 ISO/IEC Guide 98-3:2008, Uncertainty of measurement -- Part 3: Guide to the expression of uncertainty in measurement (GUM:1995)
- 2.1.3.36 ISO/IEC Guide 98-1:2009, Uncertainty of measurement -- Part 1: Introduction to the expression of uncertainty in measurement
- 2.1.3.37 P.R.Bevington and D.K.Robinson, Data Reduction and Error Analysis for the Physical Sciences, 2003.
- 2.1.3.38 L.M. Schwartz, Random Error Propagation by Monte Carlo Simulation, Analytical Chemistry, Volume 47, No. 6, pp. 963-964, May 1975.

2.2 Definitions

2.2.1 AIRCRAFT GAS TURBINE ENGINE

Any gas turbine engine used for aircraft propulsion or for power generation on an aircraft, including those commonly called turbojet, turbofan, turboprop, or turboshaft type engines, or auxiliary power units.

2.2.2 AERODYNAMIC DIAMETER

The diameter of an equivalent sphere of unit density (1 g/cm³) with the same settling velocity as the particle in question.

2.2.3 CYCLONE SEPERATOR

A device that removes particles larger than a prescribed aerodynamic diameter via inertial and gravitational means. The specified cut-point diameter is associated to the percent of particles that penetrate through the cyclone [e.g., D_{50} refers to a diameter with a 50% penetration].

2.2.4 ELECTRICAL MOBILITY DIAMETER

The diameter of an equivalent sphere with the same electrical mobility as the particle in question; also referred to as mobility diameter.

2.2.5 NON-VOLATILE PARTICULATE MATTER (nvPM)

Emitted particles at the gas turbine engine exhaust nozzle exit plane that do not volatilize when heated to a temperature of 350 °C (623.15 K).

2.2.6 NON-VOLATILE PARTICLE MASS CONCENTRATION

The mass of non-volatile particles per unit volume of sample.

2.2.7 NON-VOLATILE PARTICLE MASS EMISSION INDEX

The mass of non-volatile particles emitted per unit of fuel mass used.

2.2.8 NON-VOLATILE PARTICLE NUMBER CONCENTRATION

The number of non-volatile particles per unit volume of sample.

2.2.9 NON-VOLATILE PARTICLE NUMBER EMISSION INDEX

The number of non-volatile particles emitted per unit of fuel mass used.

2.2.10 PARTICLE SIZE DISTRIBUTION

The probability density function, list of values, or mathematical function that expresses the nvPM (number, mass, surface area, or volume) concentration according to size. Engine exhaust is comprised of particles with diameters spread over several orders of magnitude and are typically measured in terms of their electric mobility.

2.2.11 PENETRATION FRACTION

The ratio of non-volatile particle concentration entering and leaving a sampling and measurement system segment.

2.2.12 SAMPLING PROBE

The device placed in the engine exhaust plume used to extract a representative sample.

2.2.13 SEGMENT

A continuous portion of sampling line that has the same diameter, wall temperature, and flow rate.

Symbols, Acronyms, and Terminology³

2.3.1 [CO₂]

Mole fraction concentration of carbon dioxide in the engine exhaust on a wet basis.

2.3.2 [CO₂]_{dil1}

Mole fraction concentration of carbon dioxide after the first dilution stage on a wet basis ick to view the full PD

2.3.3 $C_{\rm p}$

The carrier gas constant pressure specific heat capacity.

2.3.4 CPC

Condensation Particle Counter.

2.3.5 C_c

The dimensionless Cunningham slip correction factor

2.3.6 D_{50}

The particle diameter (electrical mobility unless stated otherwise) at which 50% of particles with diameters of D₅₀ are detected; likewise D₁₀, D₁₆, D₈₄, and D₉₀ are the particle diameters at which 10%, 16%, 84%, and 90% of particles with particle diameters of D₁₀, D₁₆, D₈₄, and D₉₀ are detected, respectively, nm.

2.3.7

The particle diffusion coefficient, cm²/s.

2.3.8 DF

Dilution Factor (sample concentration before dilution)/(sample concentration after dilution).

2.3.9 DF₁

The first stage dilution factor [CO₂]/[CO₂]_{dil1}.

2.3.10 DF₂

The second stage (VPR) dilution factor as per calibration.

There are a few symbols with subscripts that differ with other E31 and ANNEX16 documents. In this AIR the underscore, " ", is not used in subscripts. This was done to avoid the equation editor misinterpretation of the underscore.

2.3.11 D_m

nvPM particle diameter refers to the electrical mobility diameter except for the cyclone separator where the particle diameter is the aerodynamic diameter, nm.

2.3.12 DMA

Differential mobility analyzer (also refer to AIR6037).

2.3.13 D_{mg}

Geometric mean diameter of an nvPM size distribution, nm.

2.3.14 δ

Square of the relative difference between the measured and calculated nvPM mass to number concentration ratios.

2.3.15 $\Delta ln(D_m)$

Width of a size bin in base natural logarithm.

2.3.16 EI

Emission index.

2.3.17 Elmass

nvPM mass emission index corrected for Probe inlet to Diluter1 (n)et thermophoretic losses, mg/kg fuel.

2.3.18 EI_{num}

nvPM number emission index corrected for Probe inlet to Diluter1 inlet thermophoretic losses, particles/kg fuel.

2.3.19 ε

Convergence criterion (1×10-9) in the method for determining the number and mass corrections.

 $2.3.20 \, f_{lgn}(D_m)$

Lognormal distribution function with parameters of geometric standard deviation, σ_g , and geometric mean diameter, D_{mg} .

2.3.21 $f_N(D_m)$

Engine exhaust nozzle exit plane nvPM number lognormal distribution function.

2.3.22 h_{gas}

Carrier gas convective heat transfer coefficient.

2.3.23 IDi

Inner diameter of the ith segment of the sampling line, cm.

2.3.24 k_B

Boltzmann constant, 1.3806 x 10⁻¹⁶ (g·cm²)/(s²·K) in cgs units.

2.3.25 kslmass

Elmass correction factor for system losses without Probe inlet to Diluter1 inlet thermophoretic loss correction for particle diameters greater than or equal to 10 nm.

2.3.26 ksLnum

El_{num} correction factor for system losses without Probe inlet to Diluter1 inlet thermophoretic loss correction for particle diameters greater than or equal to 10 nm.

2.3.27 kthermo

Thermophoretic loss correction factor for the Probe inlet to Diluter1 inlet.

2.3.28 k_{thi}

Thermophoretic loss correction factor for the ith segment, distinguished from the probe tip to biluter1 inlet thermophoretic

Carrier gas viscosity.

 $2.3.34 \mu_0$

Carrier gas viscosity at T₀ and P₀, equal to 1.83 x 10⁻⁴ g/cm·s.

2.3.35 nvPMmassUN

The undiluted (i.e., corrected for dilution) instrument nvPM mass concentration, µg/m³.

2.3.36 nvPMmi

Non-volatile particulate matter mass instrument.

2.3.37 nvPM_{numUN}

Undiluted (i.e., corrected for dilution) instrument nvPM number concentration, particles/cm³.

2.3.38 nvPMni

Non-volatile particulate matter number instrument.

2.3.39 nvPM_{massEP}

Estimated engine exhaust nozzle exit plane nvPM mass concentration.

2.3.40 nvPM_{numEP}

Estimated engine exhaust nozzle exit plane nvPM number concentration with particle diameters between 3 nm and 1000 nm used in the iterative solution.

2.3.41 nvPM_{numEP}(D_m>10 nm)

Estimated engine exhaust nozzle exit plane nvPM number concentration with particle diameters between 10 nm and 1000 nm used to determine the number system loss correction factor.

2.3.42 nvPM_{massSTP}

Measured diluted nvPM mass concentration at instrument STP condition, µg/m³.

2.3.43 nvPM_{numSTP}

Measured diluted nvPM number concentration at instrument STP condition, particles/cm³.

2.3.44 η

Penetration fraction.

2.3.45 η_{bi}(D_m)

The penetration fraction for the sampling line bend for ith segment of the sampling and measurement system at electrical mobility particle size D_m .

2.3.46 $\eta_i(D_m)$

The penetration fraction for the ith segment of the sampling and measurement system at electrical mobility particle size D_m.

 $2.3.47 \quad \eta_{mass}(D_m)$

The overall sampling and measurement system mass penetration fraction for the nvPMmi without Probe inlet to Diluter1 inlet thermophoretic losses at electrical mobility particle size D_m.

 $2.3.48 \quad \eta_{num}(D_m)$

The overall sampling and measurement system number penetration fraction for the nvPMni without Probe inlet to Diluter1 inlet thermophoretic losses at electrical mobility particle size D_m.

2.3.49 P₀

Reference pressure for carrier gas viscosity and mean free path, 101.325 kPa.

2.3.50 Pr

Carrier gas Prandtl number.

2.3.51 Qi

Carrier gas flow in the ith segment of the sampling system, slpm (temperature of 273.15 K and 101.325 kPa).

2.3.52 Re

Carrier gas Reynolds number.

 $2.3.53 \, \text{R}_{MN}(D_{mg})$

in the full P Calculated ratio of the estimated nvPM mass concentration, nvPM_{massEST}, to the estimated number concentration, $nvPM_{numEST}$, $(g/cm^3)(nm^3)=10^{-21}g$.

2.3.54 ρ

Assumed nvPM effective density, 1 g/cm3.

2.3.55 ρ_{gas}

Carrier gas density, g/cm³.

2.3.56 Sc

Carrier gas Schmidt number

 $2.3.57 \sigma_{q}$

The assumed geometric standard deviation of lognormal distribution.

2.3.58 T₀

Reference temperature for carrier gas viscosity and mean free path calculations, 296.15 K.

2.3.59 T₁

Sample segment control temperature at Diluter1 inlet, K.

2.3.60 Tegt

Performance-predicted engine exit exhaust gas temperature (used for Probe inlet to Diluter1 inlet thermophoretic loss calculations), K.

2.3.61 T_{gasi}

Carrier gas inlet temperature in the ith segment of the sampling system, K.

 $2.3.62\ T_{linei}$

Wall temperature of the ith segment of the sampling system, K.

2.3.63 TVPR

VPR operation temperature used to calculate diffusion penetration function of the VPR, K.

2.3.64 θ_{bi}

MORIN. COM. Click to view the full Pith of airosoft. Total angle of bends in the ith segment of the sampling line, degrees.

2.3.65 VPR

Volatile Particle Remover.

2.4 Units

Physical Quantities

atm = 1 standard atmosphere, 101325 Pa

cm = centimeter (10^{-2} m)

g = gram

Hz = Hertz (1 per second)

K = Kelvin

 $kPa = kilopascal (10^3 Pa)$

m = meter

 $nm = nanometer (10^{-9} m)$

 $\mu m = micrometer (10^{-6} m)$

Pa = pascal

s = second

slpm = standard liters per minute (Volumetric flow at STP condition)

STP conditions = standard temperature and pressure conditions, 273.15 K and 101325 Pa

Prefixes

 $k = kilo, 10^3$

 $h = hecto, 10^2$

 $da = deka. 10^{1}$

 $d = deci, 10^{-1}$

 $c = centi, 10^{-2}$

 $m = milli, 10^{-3}$

 $\mu = \text{micro}, 10^{-6}$

 $n = nano, 10^{-9}$

 $pico = pico, 10^{-12}$

INTRODUCTION

3.1 Background

JII PDF of air650A In contrast to gaseous emissions which have molecular properties, nvPM emissions from aircraft gas turbine engines have sizes (diameters) on the order of tens of nanometers (nm). Physically innerent with these small nvPM sizes, there is loss of particles in the sampling system that transports the exhaust sample from the probe tip to the measurement instruments.⁴ These nvPM sampling system losses occur due to a number of different physical mechanisms which change the trajectory of a particle and cause the particle to deposit on the internal surfaces of the sampling line. For particle sampling from gas turbine engines, the most significant particle losses are due to thermophoresis and diffusion. Thermophoretic losses occur when the sampling segment wall temperature is lower than the exhaust gas temperature, whereas diffusional losses are dependent on the sampling segment geometry and the exhaust sample flow rate. In the particle size range of current turbojet and turbofan aircraft engines (particle diameters <300 nm), thermophoretic losses are nearly independent of particle size, whereas diffusional losses increase with decreasing particle size. Because of the high temperatures of the aircraft gas turbine engine exhaust, the small particle size, and the length of the sampling system overall nvPM losses can be significant (size dependent particle losses on the order of 50% for nvPM mass concentration and 90% for nvPM number concentration). To account for the losses, both the size dependent penetration functions and the size distribution of the emitted particles need to be known to quantify corrections to the measured nvPM mass and number concentrations or emissions indices.

Although the direct measurement of particle size is not required, nvPM mass and number concentrations themselves can constrain the particle size distribution. For example, the average nvPM mass per particle can be estimated by dividing the known, total measured nvPM mass concentration by the known, total measured nvPM number concentration. Then, assuming that particle density is known and independent of particle size, the volume per particle is obtained by dividing the average nvPM mass per particle by the assumed density. From this volume, the diameter of a spherical particle can be calculated to obtain the mass-weighted mean spherical equivalent particle size.

Most particle size distributions are not mono-disperse, and thus have a distribution with a finite width. In fact, most particle formation mechanisms are stochastic processes that result in a lognormal distribution. This has been observed regularly for aircraft engine nvPM emissions. The non-dimensional size distribution width, the geometric standard deviation, has been fairly well determined, based on a large number of measurements [References 2.1.3.1 through 2.1.3.13]. For practical reasons, the assumption of a lognormal distribution can be used to further constrain the size distribution, and with the measured nvPM mass and number concentrations, a complete size distribution can be inferred.

⁴ The recommendations in this document build upon the methods for the loss estimations described in AIR6037.

With a theoretical size distribution determined as just described, and a measured or calculated sampling and measurement system penetration function, the system losses for a particular test condition can be assessed. In the following, the detailed approach is described with discussion of how uncertainties in the losses are related to uncertainties in the measured inputs and to the assumptions made in the present method.

3.2 Overview of the Procedure to Assess System Loss, Calculate System Penetration Functions, and Estimate Correction Factors

The system loss correction methodology is separated into two parts,

- 1. thermophoretic losses from the probe tip to the Diluter1 inlet of the sampling system and
- 2. all other sampling and measurement system losses from the probe tip to the measurement instruments.

The probe tip to the Diluter1 inlet thermophoretic losses, k_{therm} , is determined from the engine exhaust temperature, T_{EGT} , at the probe and the sample segment control temperature at Diluter1 inlet, T_1 .

For all other system losses, the ratio of the mass to number concentrations measured from the nvPM mass and number instruments are used along with nvPM particle loss penetration fractions and other factors and assumptions, discussed below, to generate a lognormal size distribution at the engine exhaust nozzle exit. This exhaust nozzle exit plane size distribution is determined by an iterative procedure that varies the size distribution geometric mean diameter. Once the size distribution is determined, both mass and number system loss correction factors, k_{SLmass} and k_{SLnum} , respectively, are determined from the ratios of the exit plane lognormal distribution to the mass line loss adjusted nvPM size distribution and the number line loss adjusted nvPM size distribution.

Finally, the measured nvPM mass and number concentrations are multiplied by $k_{therm} \times k_{SLmass}$ and $k_{therm} \times k_{SLnum}$, respectively, to estimate the exhaust nozzle exit plane nvPM mass and number concentrations. Uncertainties in the exhaust nozzle exit plane nvPM concentrations are associated with uncertainties in the sampling and measurement system losses, instruments, the assumed density, ρ , the assumed geometric standard deviation, σ_g , and the validity of the exhaust nozzle exit plane lognormal assumption.

The quantification of particle losses in the sampling and measurement system needs to take into consideration the size (diameter) of the particles because the loss mechanisms are particle size (diameter) dependent. Each loss mechanism is typically quantified in terms of the fraction of particles of a given size (i.e., particles with a given diameter, D_m) that penetrate through the sampling and measurement system. The nvPM number concentration measured at the instrument and corrected for all dilutions (DF₁ at diluter1 and DF₂ at Diluter2 in the VPR) is calculated as nvPM_{num}(D_m) = DF₁ × DF₂ × nvPM_{numSTP}(D_m). The ratio of this concentration to the concentration at the exhaust nozzle exit plane is referred to as the number penetration fraction function $\eta(D_m) = nvPM_{num}(D_m)/nvPM_{numEP}(D_m)$. The penetration fraction function may be described either as a set of penetration fractions corresponding to a set of particle diameters or as a continuous function. The penetration for nvPM mass uses similarly defined size dependent loss functions.

3.3 Note on Particle Diameters

A distinction must be made when referring to particle diameters. Particle diameters are not a unique characteristic of individual particles unless they are unit density spheres. Engine exhaust particles are usually complex agglomerates and many equivalent diameters may be defined, including for example volume equivalent diameter, projected area equivalent diameter, electrical mobility diameter, and aerodynamic diameter. The responses for the instruments used to measure nvPM mass are size independent. The lower size cutoff characteristics of the condensation particle counter used for measuring nvPM number are defined in terms of electrical mobility diameter. The most commonly used instruments for sizing gas turbine particles also measure size by electrical mobility diameter. In contrast, the penetration through the cyclone separator and sample line bends depend on aerodynamic diameter. The cyclone separator performance, as is done here, can be approximated with the mobility diameter. Thus, for the purposes of this AIR we have assumed that the aerodynamic diameter is the same as the mobility diameter.

3.4 Particle Size Distribution

nvPM size (diameter) distributions are polydisperse and depend on the nvPM source. When plotted against particle diameter, nvPM mass and number size distributions differ. Figures 1 and 2 illustrate nvPM number and mass size distributions, respectively, at three different aircraft engine power settings. The particle diameter range of interest is divided up into size bins, equally separated in log-diameter space. These distributions are an important consideration for both nvPM mass and number concentration loss assessment. The engine exhaust nozzle exit plane nvPM mass concentration, nvPM_{massEP}(D_m) in the bin at diameter D_m , is determined from the effective density, ρ , of the particles, the nvPM number concentration of particles at that diameter, nvPM_{numEP}(D_m), and an assumed equivalent spherical shape,

$$nvPM_{massEP}(D_m) = nvPM_{numEP}(D_m) \times \frac{\pi \rho D_m^3}{6}$$
 (Eq. 1)

Because of the cubic dependence of mass on diameter, the peaks in the mass distributions are shifted to larger sizes compared to the peaks in the number distributions.

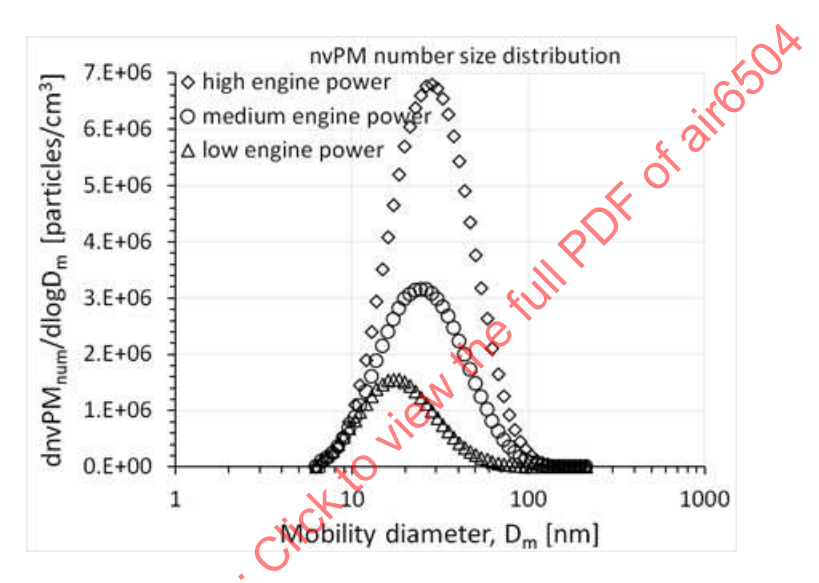


Figure 1 - Downstream nvPM number size distribution measured [Reference 2.1.3.11] after dilution at the end of the 25 m line in a AIR6241 [Reference 2.1.1.1] compliant sampling system⁵

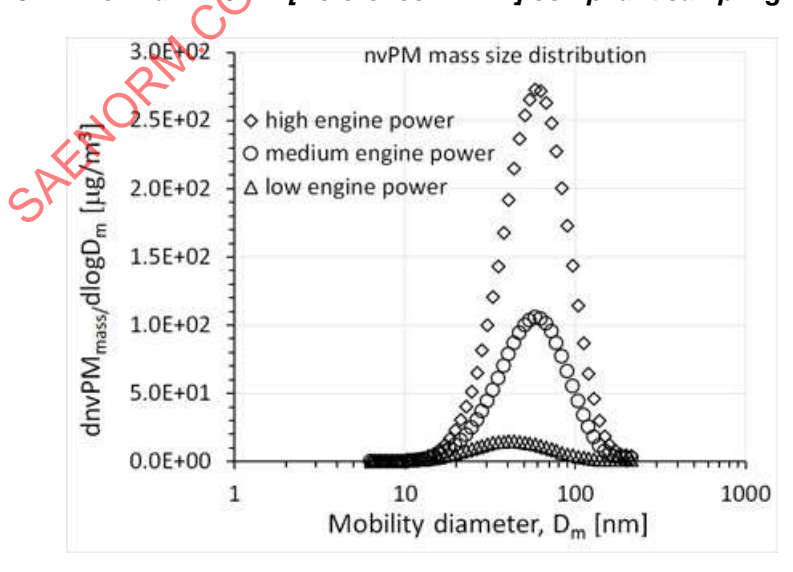


Figure 2 - Downstream nvPM mass size distribution determined from the nvPM number size distribution in Figure 1 using a density of 1 g/cm³

⁵ Typically, particle size distributions are plotted on a log base 10 scale.

3.5 Correction Method Overview

A lognormal nvPM number size distribution is defined by three parameters: width (geometric standard deviation), geometric mean diameter, and nvPM number concentration. As indicated in Equation 1, nvPM effective density links nvPM mass concentration to the nvPM number size distribution. In order to determine the corrections due to particle losses without a size measurement this method assumes a lognormal nvPM size distribution at the engine exhaust nozzle exit plane with an empirically determined geometric standard deviation and particle density. The method iteratively determines the geometric mean diameter of the distribution such that, when the distribution is multiplied by the size dependent sampling system, cyclone separator, and VPR penetration functions and the CPC counting efficiency function, the calculated nvPM mass to nvPM number ratio is equal to the measured nvPM mass to nvPM number ratio. It assumes that the nvPM mass only experiences sampling system and cyclone separator losses while the nvPM number concentration is also reduced by losses in the VPR and by the CPC counting efficiency.

Using a numerical minimization routine, the solution is obtained iteratively by adjusting the geometric mean diameter, D_{mg} , of the particle lognormal size distribution to reduce, δ , the square of the relative difference between calculated and measured ratios of mass to number, to zero. This is illustrated in Figure 3. The nvPM mass and number concentrations are obtained by integrating Equation 1 from 3 to 1000 nm.⁶ All of this is done internally by the calculation tool computer software. Once the mean particle size, D_{mg} , is determined, the nvPM mass and nvPM number system correction factors, k_{SLmass} and k_{SLnum} , respectively, are determined from the ratios of calculated exit plane nvPM mass and number to calculated instrument nvPM mass and number concentrations, i.e.,

$$k_{SLmass} = \frac{nvPM_{massEP}}{k_{thermo} \times DF_1 \times nvPM_{massSTP}} = \frac{\sum_{D_m > 1000nm}^{D_{1000nm}} \frac{\rho \pi D_m^3}{\epsilon} \times nvPM_{numEP} \times f_{lgn}(D_m) \times \Delta \ln(D_m)}{k_{thermo} \times \sum_{D_m > 3nm}^{1000nm} \eta_{thermo} \times \eta_{mass}(D_m) \times \frac{\rho \pi D_m^3}{\epsilon} \times nvPM_{numEP} \times f_{lgn}(D_m) \times \Delta \ln(D_m)}$$

$$= \frac{\sum_{D_m > 10nm}^{1000nm} D_m^3 \times f_{lgn}(D_m) \times \Delta \ln(D_m)}{\sum_{D_m > 3nm}^{1000nm} \eta_{mass}(D_m) \times D_m^3 \times f_{lgn}(D_m) \times \Delta \ln(D_m)}$$

$$= \frac{nvPM_{numEP}}{k_{thermo} \times DF_1 \times DF_2 \times nvPM_{numSTP}} = \frac{\sum_{D_m > 10nm}^{1000nm} nvPM_{numEP} \times f_{lgn}(D_m) \times \Delta \ln(D_m)}{k_{thermo} \times D_m > 3nm} \eta_{thermo} \times \eta_{num}(D_m) \times nvPM_{numEP} \times f_{lgn}(D_m) \times \Delta \ln(D_m)}$$

$$= \frac{\sum_{D_m > 10nm}^{1000nm} \eta_{lgn}(D_m) \times \Delta \ln(D_m)}{\sum_{D_m > 3nm}^{1000nm} \eta_{lgn}(D_m) \times \Delta \ln(D_m)}$$

$$= \frac{\sum_{D_m > 10nm}^{1000nm} f_{lgn}(D_m) \times \Delta \ln(D_m)}{\sum_{D_m > 3nm}^{1000nm} \eta_{lgn}(D_m) \times \Delta \ln(D_m)}$$
(Eq. 3)

In these equations the exit plane number concentrations, nvPM_{numEP}, cancel in the numerators and denominators leaving ratios of the sum of the engine exit plane size distributions to the sum of the system loss adjusted nvPM size distributions for either mass or number. Note that the thermophoretic loss penetration factor, η_{thermo}, of the Probe inlet to Diluter1 inlet in Sections 1 and 2 and loss factor, k_{thermo}, are separated out of the calculation based on AIR6241 requirements [Reference 2.1.1.1].

The nvPM number and mass correction factors only consider particles larger⁷ than 10 nm in the calculation for the exit plane nvPM number concentration, but considers particles 3 nm and above for the estimated measured nvPM number concentration because that is what the instruments will actually measure. Note that the system penetration functions drop to zero rapidly near 10 nm, making it unlikely that particles less than 10 nm get counted.

⁶ This size range reflects the submicron nature of aerosols generated by aircraft gas turbine engines.

⁷ This is due to the large uncertainties in particle number measurements below 10 nm.

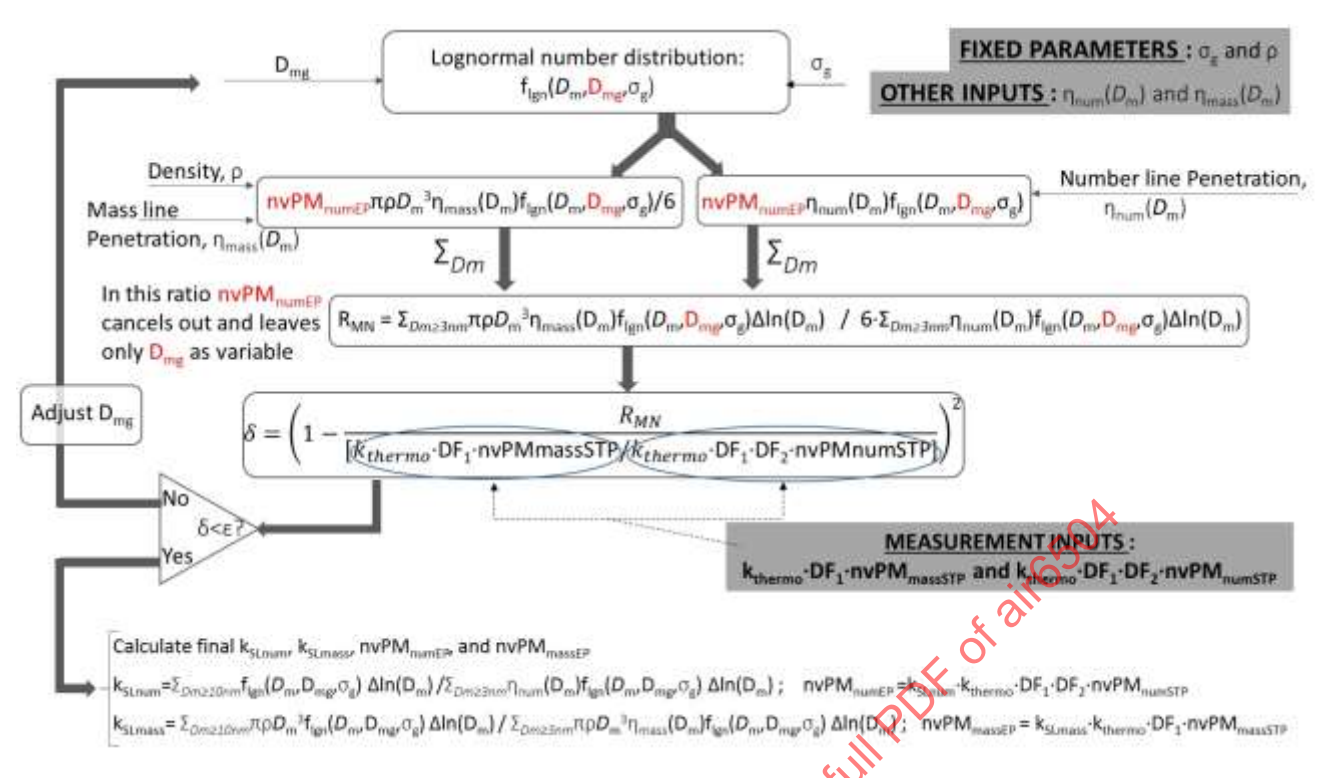


Figure 3 - Correction method diagram. Note that k_{thermo} and DF_T cancel out and hence have no impact on the calculations. These equations are expressed in more detail in Equations 28 and 29.

Engine exhaust exit plane nvPM mass and number concentrations are calculated iteratively in this method from the loss and dilution corrected measured nvPM mass and number concentrations at their respective instruments using the sampling and measurement system penetration fractions. Correction factors, k_{SLnum} and k_{SLmass}, for nvPM mass and number, respectively, are the ratios of the engine exhaust exit plane nvPM mass and number concentrations calculated by the method to the loss and dilution corrected measured nvPM mass and number concentrations. More explicitly, the nvPM mass and number correction factors are defined by the following equations,

$$nvPM_{numEP} = k_{SLnum} \times k_{thermo} \times DF_1 \times DF_2 \times nvPM_{numSTP}$$
 (Eq. 4)

$$nvPM_{massEP} = k_{SLmass} \times k_{thermo} \times DF_1 \times nvPM_{massSTP}$$
 (Eq. 5)

This is explained with more detail in Appendix B.

4. SYSTEM PENETRATION CALCULATIONS

4.1 Required Parameters to Determine System Losses

The correction method described in Section 3 requires parameters from the sampling system, instrument calibration results and test measurements. How these parameters are determined is described in Sections 5, and 6. It does not require any additional measurements beyond those specified in AIR6241 [Reference 2.1.1.1].

4.2 Measured nvPM Mass and Number

Table 1 - Measured nvPM mass and number parameters necessary for system loss correction calculations

Parameter Symbol	Description	Units
nvPM _{massSTP}	diluted nvPM mass concentration at instrument STP condition	μg/m³
nvPM _{numSTP}	diluted nvPM number concentration attributed nvPM number concentration	particles/cm ³
DF ₁	first stage dilution factor, [CO ₂]/[CO ₂] _{dil1}	-
DF ₂	second stage (VPR) dilution factor as per calibration	-

4.3 United Technologies Research Center (UTRC) Line Penetration Function Calculation Method

In 2008, a spreadsheet was developed at UTRO [References 2.1.3.12, 2.1.3.13, and 2.1.3.14] to predict particle transport as a function of particle size which could then be used to assess the performance of various sampling line configurations. The resulting Excel-based tool [References 2.1.1.1 and 2.1.1.2] assumes steady state flow and calculates particle losses using standard equations taken from yook and Pui [Reference 2.1.3.14] and Willeke and Baron [Reference 2.1.3.15]. Although Baron created a very powerful and widely used spreadsheet tool called Aerocalc [Reference 2.1.3.16] that contains many of the same particle transport calculations, Aerocalc treats each loss mechanism as a separate calculation. The UTRC tool has simplified the analysis of a sampling system by combining the effect of up to five different particle loss mechanisms: turbulent diffusional, inertial, bends, thermophoretic, electrostatic and allows definition of up to 10 different sampling system Sections and segments. The loss calculation tools developed for this document extends the 10 segments in the UTRC tool to 15 discrete segments.

Flow characteristics such as velocity, Reynolds number, and Stokes number are closely coupled to gas and particle properties. The expressions given for penetration efficiency due to each specific loss mechanism are under conditions assumed to be steady for a steady engine operation point. Velocity, temperature and pressure within a single segment of transport line of constant diameter and wall temperature will result in a single efficiency value for a single physical loss mechanism.

The UTRC tool predicts transport efficiency for particles over a range of sizes, based on characteristics of the flow, the transport line and ambient conditions for temperature and pressure. The UTRC tool does not account for coagulation, which, in some cases, can affect nvPM size and number (see 7.1.3). The equations implemented in these tools for various loss mechanisms are steady state expressions [References 2.1.3.12 through 2.1.3.25] as listed in 4.5 through 4.11 and in Appendix A.

When considering the sampling and measurement system for which this AIR6504 is written, the parameters which must be defined for each system section are listed in Table 2. For reference Figure 4 is a schematic of the sampling system defined in the AIR6241 [Reference 2.1.1.1].

Additional parameters that are required for the sampling and measurement system loss calculations are shown in Table 3. Although these parameters can be modified for a different carrier gas or particle description, the values for the carrier gas and particle properties are fixed to match air. In addition, the displayed size range is tailored to the D_{50} (=1000nm) of the cyclone separator. However, the calculations are valid to 10000 nm.

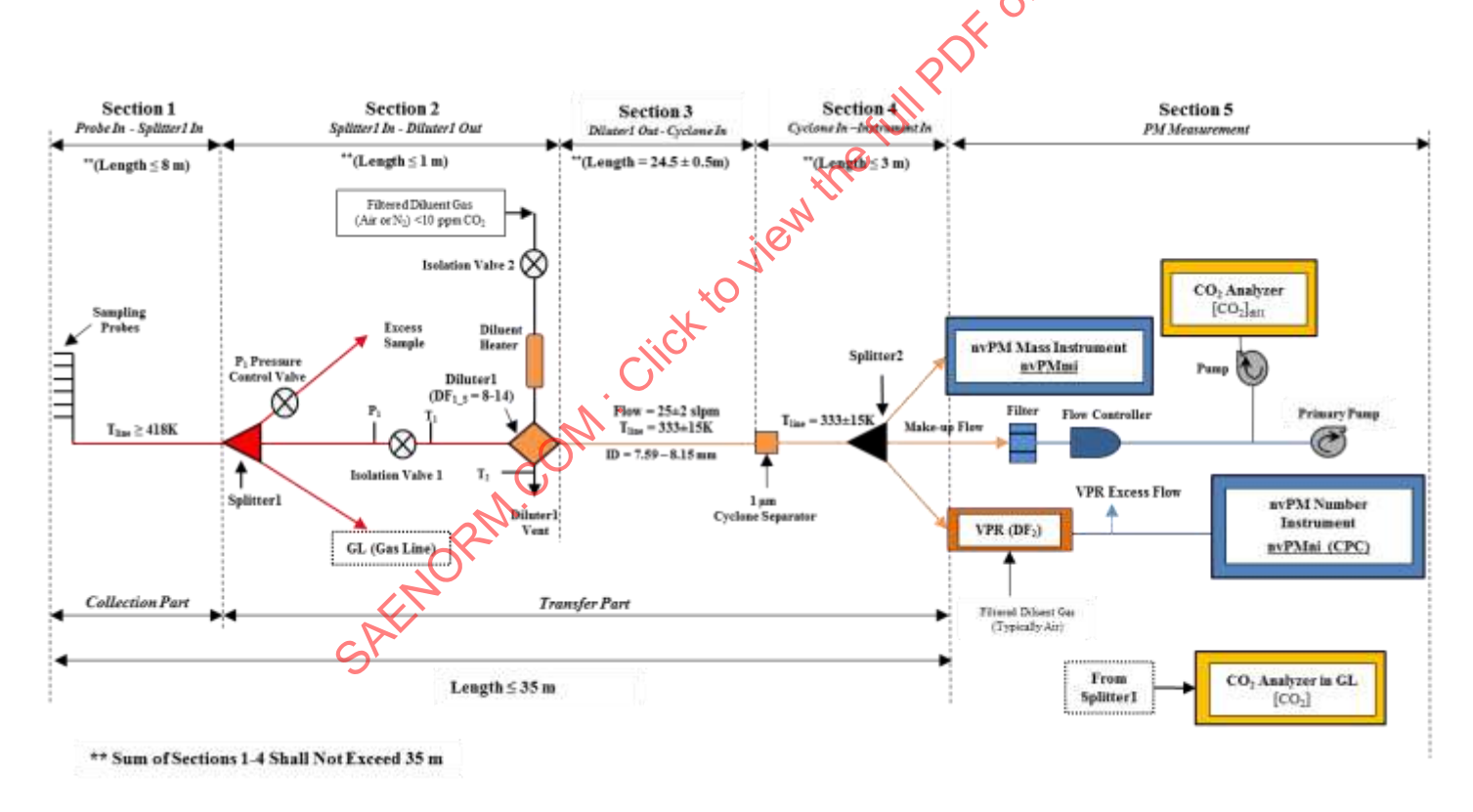


Figure 4 - nvPM sampling and measurement system diagram defined in AIR6241 [Reference 2.1.1.1]

Table 2 - Sampling and measurement system input parameters8

Parameter		
Symbols	Descriptions	Units
T _{gasi}	Temperature of the carrier gas of i th segment of the sampling line. (This is typically the line segment wall control temperature, T _{linei} , except when two adjoining segments differ in temperature. See Appendix A.1 for further explanation.)	К
T _{linei}	Line segment wall control temperature of the i th segment of the sampling line	K
T _{EGT}	Performance-predicted engine exit exhaust gas temperature	K
Pi	Pressure of the carrier gas in the i th segment of the sampling line, assumed constant throughout the i th segment and equal to 101.325 kPa	kPa
Qi	Flow rate of the carrier gas through the i th segment of the sampling line (Collection Part segment flow rates are estimated)	slpm
IDi	Inside diameter of the i th segment of the sampling line	cm
Li	Length of the i th segment of the sampling line	cm
θ_{bi}	Total angle of bends in the i th segment of the sampling line	degrees
ηνρκ(15),	VPR penetration fractions at particle diameters of 15 nm, 30 nm, 50 nm and	dimensionless
ηνρκ(30), ηνρκ(50), ηνρκ(100)	100 nm which are used to determine the VPR penetration function	
η _{CPC} (10), η _{CPC} (15)	CPC counting efficiency at particle diameters of 10 nm and 15 nm which are used to determine the CPC counting efficiency function	dimensionless
cyclone separator D ₅₀	Cyclone separator particle diameter at which 50% of particles diameters of D ₅₀ are detected which is used to determine the cyclone separator penetration function	nm
cyclone separator sharpness, (D ₁₆ /D ₈₄) ^{0.5}	Ratio of cyclone separator particle diameters at which 16% and 84% of particles with diameters of D ₁₆ and D ₈₄ traverse from cyclone separator inlet through cyclone separator outlet which is used to determine the cyclone separator penetration function	dimensionless

Table 3 - Carrier gas and particle properties used in the particle transport calculations

Carrier Gas Properties	Value 📣	Units	Notes
composition	air _O	-	
viscosity, μ ₀	0.000183	g/cm•s	Evaluated at 296 K and 101 kPa, not at STP
	all.		temperature conditions
mean free path, λ ₀	67.3	nm	Evaluated at 296 K and 101 kPa, not at STP
الم	J		temperature conditions
Particle properties	Value	Units	Notes
Density	1	g/cm ³	Assumed effective density
thermal conductivity 0.2		W/m•K	Assumed thermal conductivity
size range 3 to 1000		nm	particle diameter

NOTE: These sampling system parameters for the individual sections of the sampling and measurement system in Figure 4 can be subdivided into segments to be defined more accurately. The net penetration function for any section of the sampling and measurement system is the product of all the penetration functions defined for that section.

4.4 Note on Penetration Measurements

Measurement of penetration fractions for sampling systems is difficult. "While most physical loss processes have been described relatively accurately, the practical assessment of aerosol sampling systems is, in general, more complicated because often several loss processes interact. Common practices to characterize the performance of aerosol inlets include calibration experiments using test aerosols, and numerical simulations using computational fluid dynamics and aerosol dynamics models." [Reference 2.1.3.17] Because of the difficulty of these measurements and the associated uncertainties, the calculated penetration fractions described in this document are considered more robust.

4.5 Calculation of Penetration Functions

The size dependent transport efficiency, also called penetration efficiency, is the probability that a particle of a given size that enters the line, exits the line. For a certain size, nvPM mass and number are related. Because number concentrations are sufficient to measure the nvPM size distribution, the penetration efficiency is calculated on nvPM number concentration.

The nvPM sampling and measurement system is composed of multiple segments each having its own penetration efficiency, η_i . Each of these can be multiplied together to give a total penetration efficiency for that segment for particles of a given diameter, where the penetration efficiency through each segment is represented as η_1 , η_2 , η_3 , ..., η_n . The sampling and measurement system overall penetration efficiency (η_n) is the product of all the segment efficiencies:

$$\eta_p = \prod_{i=1}^n \eta_i = \eta_1 \times \eta_2 \times \eta_3 \dots \times \eta_n$$
 (Eq. 6)

The subscripts refer to a component or segment of the sampling system as listed in Table 4. Hence, the penetration functions for the nvPM mass transport and nvPM number transport lines are,

$$\eta_{mass}(D_{m}) = \eta_{1} \times \eta_{b1} \times \eta_{th1} \times \eta_{2} \times \eta_{b2} \times \eta_{th2} \times \eta_{3} \times \eta_{b3} \times \eta_{th3} \times ... \times \eta_{cyc}$$
 (Eq. 7)

$$\eta_{num}(D_m) = \eta_1 \times \eta_{b1} \times \eta_{th1} \times \eta_2 \times \eta_{b2} \times \eta_{th2} \times \eta_3 \times \eta_{b3} \times \eta_{th3} \times \dots \times \eta_{cyc} \times \eta_{VPR} \times \eta_{CPC}$$
 (Eq. 8)

where η_{mass} and η_{num} are the product of the penetrations over the total number of mass or number sample line segments, respectively.

Figure 5 illustrates, for a typical system, the VPR penetration function, η_{VPR} , the CPC counting efficiency, η_{CPC} , and the penetration functions for, η_{mass} and η_{num} , at the nVPM mass and number instruments (excluding Probe inlet to Diluter1 inlet thermophoretic losses, η_{thermo} , in Sections and 2), respectively. The individual penetration functions, η_i , are defined in Table 4 and discussed more thoroughly in 4.6 through 4.11 and in Appendix A.

Implementation Notes

- The nvPM sampling system should be subdivided into segments. The number of segments will depend upon the specific probe and sampling system used. A new segment shall be defined based on a change of one of the following parameters: sample flowrate, sample line control wall temperature or sample line ID >15%.
- 2. Since the Probe inlet to Diluter1 inlet thermophoretic loss in the sampling and measurement system are done separately and outside of the loss correction tools, the segments used to construct the probe inlet to Diluter1 inlet of the sampling and measurement system should equate the wall temperature with the gas temperature of each segment. However, from the Diluter1 outlet to the instrument inlets, actual sample gas and segment line wall temperatures should be used. In practice, temperature differences will occur if an upstream segment line wall temperature is higher than the next adjoining downstream segment line wall temperature. At the date of this AIR publication this has only been observed at the mass instrument inlet. The standard input data set has an example of how this is handled in segment numbers 1 through 5, and the mass line segment number 11. In Figure 6 these temperatures are highlighted in blue.

3. The estimated sample flowrate through the Collection Part will change with engine thrust setting. For a specific engine test, if the difference between using the lowest estimated flowrate and highest estimated flowrate has an impact of less than 1% on the system loss correction factors for both nvPM mass and number, then a single estimated Collection Part sample flowrate can be assumed for all system loss correction factor calculations for that engine test. Otherwise the individual estimated flowrates should be used per engine test point system loss calculation.

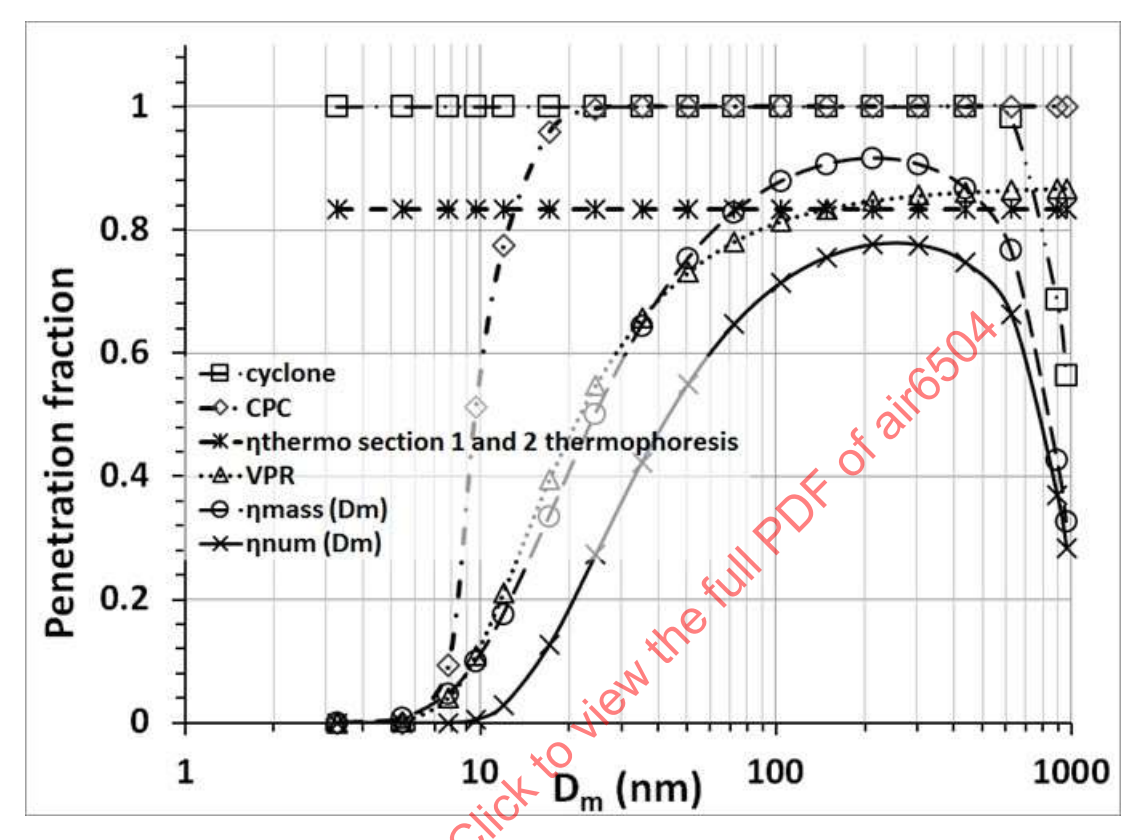


Figure 5 - Mass and number penetration functions from a single tip probe to the nvPM mass and number instruments. The mass penetration function is determined from the cyclone separator penetration and the UTRC model of diffusional and bend losses. The number penetration function includes the UTRC diffusional and bend losses, the cyclone separator penetration function, the VPR penetration function, and the CPC penetration efficiency. Also illustrated are the counting efficiency curve for the CPC, the VPR penetration curve, and the thermophoretic loss of Sections 1 and 2. (Neither the mass or number penetration functions include the thermophoretic loss from the Probe inlet to Diluter1 inlet of Sections 1 and 2.)

Table 4 - nvPM Sampling and measurement system component and segment penetration fractions. In the loss calculation software tools, there are up to fifteen line penetration segments, η_i , available that can be used to construct continuous, individual mass and number segment line penetrations, η_{mass} and η_{num} , from the probe inlet to the mass and number instruments. Each segment line penetration, η_i , will have a diameter, ID_i , wall temperature, T_{linei} , sample gas temperature, T_{gasi} , and sample flow rate, Q_i , and will be used to compose the 5 sampling system sections. If fewer than fifteen segments are required to describe the sampling system, the lengths of the unused segments must be set to have zero length and identical wall and gas temperatures. The tools will then ignore the penetration contributions of these segments.

Parameter	
Symbol	Description
η _i (D _m)	Segments i=1 to 15, Probe inlet to instrument inlet
η _{bi} (D _m)	Segments i=1 to 15, Probe inlet to instrument inlet for bends
η _{dil} (D _m)	Diluter1
η _{cyc} (D _m)	Cyclone separator
η _{thi}	Segment thermophoretic losses; the thermophoretic loss for the sampling system from the sample probe to the Diluter1 outlet is determined separately from the Diluter1 outlet to the instrument inlets thermophoretic losses; see Note in this section and see Appendix A
$\eta_{VPR}(D_m)$	nvPMni VPR
η _{CPC} (D _m)	nvPMni CPC counting efficiency

NOTES:	individual probe	ganged probe arm	ganged probe	probe exit to Splitter1	Splitter1 inlet to Diluter1 inlet	Diluter1 inlet	Diluter1 inlet to 25m line	25meter line to Cyclone Seprator and Splitter2	diluter	APC diluter	Splitter2 to nvPMmi	not used	not used	not used	not used	
N.				Sami	oling Lin	e Input P	aramete	rs								
Segment ->		1	2	3	4 ×	9 5	6	7	8	9	10	11	12	13	14	15
Segment carrier gas temperature, Tgasi	K	750	750	433	de	433	333	333	333	333	333	333	273	273	273	273
Segment pressure, P0	kPa	101.33	101.33	101.33	101.33	101.33	101.33	101.33	101.33	101.33	101.33	101.33	101.33	101.33	101.33	101.33
Segment flowrate, Qi	slpm	4.17	12.50	12.50	50.00	2.50	2.50	25.00	25.00	4.50	4.50	3.45	0.00	0.00	0.00	0
Segment Tube Diam, IDi	cm	0.150	0.435	0.775	0.775	0.775	0.099	0.775	0.775	0.400	0.400	0.400	0.800	0.800	0.775	0.775
Segment Length, Li	cm	5.0	100%	200.0	400.0	26.7	1.4	56.3	2499.4	170.2	15.9	134.6	0.0	0.0	0.0	0.0
Segment line temperature, Tlinei	K	750	750	433	433	433	333	333	333	333	333	303	273	273	273	273
Segment bends, Obi	degrees	O.M.	260	380	210	0	0	0	1170	250	0	230	0	0	0	0
Mass/Number Flag	String	вотн	вотн	вотн	ВОТН	вотн	вотн	вотн	вотн	NUMB	NUMB	MASS	BOTH	ВОТН	вотн	BOTH

Figure 6 - An example of a thermophoretic loss occurring at the mass instrument inlet. In this case, the mass instrument inlet line wall temperature is controlled to 303 K and the line wall temperature of segment 11 is controlled to 333 K. Thermophoretic loss will occur in the instrument inlet line. Hence, the gas temperature of segment 11 is set to 333 K and the segment 11 wall temperature is 303 K. The probe inlet to Diluter1 inlet thermophoretic loss is determined outside of the loss tool. Hence, segments 1 through 5 all have identical carrier gas and line temperatures.

⁹ Some of these sections, of course, can be subdivided further into segments of a given sampling system section.

4.6 Diffusional, Thermophoretic, and Bend Penetration Fractions from the UTRC Model

The loss correction factor calculation tools (Excel® spreadsheet tool with Visual Basic calculators and MATLAB® tool) all contain the standard equations used to determine nvPM transport efficiencies or penetration fractions that result from diffusional, thermophoretic, and inertial (due to bends) losses of particles onto the surface of the sampling system line walls. These tools allow for a straightforward calculation of the penetration functions for each line length depending on the sample or carrier gas flow, line inner diameter, line length, line bend angles, line temperature, gas temperature, and a few other parameters already input into the tools. Examples of these calculations are given in Section 8. The next two sections give an overview of these diffusional penetration equations. More details are given in the Appendix A and in [References 2.1.3.12 through 2.1.3.25].

In the following sections there are distinctions made between laminar and turbulent based models used to calculate losses. The decision on which model (turbulent rather than laminar) to use is empirically based. The turbulent model penetration fractions compare better with measured penetration fractions.

4.6.1 Segments up to the Instrument Inlets, $\eta_i(D_m)$, i=1, 2, 3, ..., 15

In the UTRC spreadsheet diffusional losses are modeled with standard models of particle diffusion in a turbulent flow. This will hold for all sampling system flows up to the instrument inlets. Penetration values, nice, of diffusional losses in these segments are calculated with the expression

$$\eta_i(D_m) = e^{\frac{-\pi I D_i L_i V_{d,diff}}{Q_i}}$$
 (Eq. 9)

where V_{d,diff} is the deposition speed, ID_i and L_i are the sampling line inner diameter and length, respectively, and Q_i is the gas flow in the ith sampling line segment. A more detailed discussion of this expression is given in the Appendix A.

Penetration fractions at 80 discrete particle sizes (D_m) in the range from 3 to 1000 nm should be calculated for diffusional losses as applicable for each segment and component of the sampling and measurement system.

4.7 Penetration Fractions Due to Inertial Particle Losses in Bends from the UTRC Model, ηρί(Dm)

Bends in a sampling line cause losses due to the redirection of the flow from a straight path. Although these losses are dependent on the degree (a larger bend angle will yield more losses 10), they are also dependent on the sum of the bend angles in a sampling system, since the redirection of the flow from a straight path by a tube bend causes particles to impinge on the wall of the tube beyond diffusional losses occurring in a straight sample tube.

In contrast to the diffusional losses, sampling system bend penetration fractions are distinguished for turbulent flow, Re is greater than 5000, and laminar flow, Re is less than or equal to 5000 where Re is the Reynolds number. For laminar flow (including the transition regime, Re ≤5000) the penetration due to bends in the transport lines should be calculated as

$$\eta_{\rm bi} = 1 - 0.01745 \times \text{Stk} \times \theta_{\rm bi} \tag{Eq. 10}$$

AIR6037 recommends all bends have a radius of curvature greater than 10 tube diameters and that any bend in Section 3 (i.e., the 25 m line) has a minimum coiled radius of 0.5 m (radius of curvature ~60 tube diameters). Although this stipulation helps to reduce the bend losses, it does not remove losses due to wall collisions caused by bends redirecting the sample flow.

For turbulent flow (Re >5000) the penetration due to bends in the transport lines should be calculated as

$$\eta_{bi} = e^{-0.04927 \times Stk \times \theta_{bi}} \tag{Eq. 11} \label{eq:eta_bi}$$

where:

 θ_{bi} = total angle of bends in the ith segment of the sampling line in degrees

Stk = dimensionless Stokes number

$$Stk = \frac{Q_{i} \times C_{c} \times \rho \times D_{m}^{2} \times 10^{-3}}{27 \times \pi \times \mu \times 1D_{i}^{3}}$$
 (Eq. 12)

Penetration fractions at 80 discrete particle sizes (D_m) in the range from 3 to 1000 nm should be calculated for bend losses as applicable for each segment of the sampling and measurement system.

When counting individual bends in a flexible sampling line, each bend should be measured to a 10° resolution. In Section 5, if there is a flexible sampling line between VPR inlet and CPC inlet, then the total bend of this sampling line should be added to the total bend of the Section 4 segment to VPR inlet with Section 5 bend penetration calculated as part of the Section 4 segment.

4.8 Thermophoresis

In addition to the diffusive behavior of particulate transport, convective flow due to thermal gradients in sampling lines cause particle losses to the inner walls of sampling system line segments and components. Thermal gradients caused by line temperatures which are lower than gas temperatures cause additional particle deposition onto the sampling line inner surfaces. The UTRC spreadsheet uses the thermophoretic expression [References 2.1.3.18 and 2.1.1.3] that is dependent on the sampling system segment wall temperatures, T_{linei} and sample system segment gas temperature, T_{gasi}. For a given sampling system set-up the gas and particle properties can be assumed approximately constant. Additionally, sampling lines are sufficiently long (>>10 cm) for the gas and particles to thermally equilibrate with the sampling line wall temperature. Hence, except where the sample initially enters the system, thermophoretic losses will take place only when two connecting segments are at differing temperatures, T_{wallupstream} and T_{walldownstream}, and the upstream segment is at a higher temperature than the segment directly downstream of it (T_{walupstream}>T_{walldownstream}). The thermophoretic loss will take place in the downstream segment whereby upstream gas temperature is equilibrated to the lower downstream gas temperature.

For the specific case of the thermophoretic loss from the Probe inlet to Diluter1 inlet, a simplified loss equation shall be used. It uses the segment wall temperature and the inlet gas temperature. In this simplified equation, the thermophoretic loss relationships have been shown [References 2.1.1.3 and 2.1.3.18] to reduce to:

$$\eta_{thermo} \approx \left[\frac{T_{exit}}{Tin}\right]^{constant}$$
(Eq. 13)

where T_{in} is the temperature of the gas entering the sampling line which is approximately the engine exhaust temperature, i.e., $T_{in} \approx T_{EGT}$, T_{exit} is the equilibrated sample particulate and gas temperature which is approximately the temperature of the sampling line wall (the diluter inlet wall temperature, T_1), $T_{exit} \approx T_{wall} (=T_1)$, and the exponential constant¹¹ is equal to 0.38. Hence, the thermophoretic penetration fractions for the segment 1 and 2 aircraft turbine engine work are assumed to follow:

$$\eta_{thermo} = \left(\frac{T1}{T_{EGT}}\right)^{0.38} \tag{Eq. 14}$$

where:

 $T_1 = 433.15$ K or is the measured Diluter1 inlet temperature, T_1

 T_{EGT} = engine exhaust gas temperature (in Kelvin)

Note that if $T_{EGT} \le T_1$, then $\eta_{thermo} = 1$. This Probe inlet to Diluter1 inlet thermophoretic penetration factor, η_{thermo} , has been separated from the other sampling system penetrations based on AIR6241 requirements [Reference 2.1.1.1].

If there are thermophoretic losses in other sections of the sampling and measurement system, the thermophoretic penetration fractions are determined from the UTRC thermophoretic expressions. These are explicitly shown in Appendix A, Equations A.1 and A.2. For two adjoining segments the downstream sample gas inlet temperature, T_{gasi} , is assumed to be the upstream sample segment wall temperature, i.e., $T_{gasi} = T_{wallupstream}$. The wall temperature, $T_{line} = T_{walldownstream}$, is the wall temperature of the downstream segment. There will be a thermophoretic correction needed, if the upstream segment wall temperature is greater than the downstream wall temperature, i.e., $T_{wallupstream} > T_{walldownstream}$ (see also Figure 6).

4.9 Diluter1 Penetration Fraction

A constant Diluter1 penetration, $\eta_{dil}(D_m) = 1$ should be used for all particle sizes [Reference 2.1.3.26].

4.10 Splitter Penetration Fractions

For all system splitters a constant penetration, $\eta(D_m) = 1$ should be used for all particle sizes. (Losses due to bends in the splitters should be considered using the bend equations in 4.7.)

4.11 Cyclone Separator and VPR Penetration Functions and CPC Counting Efficiencies

The loss calculation requires continuous functions for the penetration functions of the VPR and the cyclone separator and the CPC counting efficiency. This section discusses how to obtain continuous functions for the VPR, cyclone separator, and CPC used in AIR6241 [Reference 2.1.1.1] compliant sampling and measurement system from the sampling and measurement system penetration and counting efficiency values.

Using these performance specifications along with a specified analytic function, a continuous function for the penetration or counting efficiency can be determined by using a fitting routine. The functions and illustrations of the fits to the four point performance specifications for the VPR, the two point CPC specification, and specifications for the cyclone separator cutoff are described below.

¹¹ See Appendix A and Kittelson and Johnson [Reference 2.1.1.3] for a more complete discussion of the details and assumptions of this simplification.

4.11.1 Cyclone Separator Penetration Function, η_{cyc}

The minimum specifications for the cyclone separator are its sharpness (see below) and its particle aerodynamic diameter at the 50% penetration point, D_{50} . The sharpness is defined as the square root of the ratio of the particle aerodynamic diameter at 16% penetration, D_{16} , to the particle aerodynamic diameter at 84% penetration, D_{84} , i.e., $(D_{16}/D_{84})^{0.5}$. The minimum specifications for these are quantities are:

- 1. $D_{50}=1000 \pm 100 \text{ nm}$
- 2. Sharpness, (D₁₆/D₈₄)^{0.5}<=1.25

These cyclone separator sharpness and D₅₀ values are the two parameters which define the cyclone separator penetration function [References 2.1.3.27 through 2.1.3.30],

$$\eta_{cyc}(D_m) = 1 - \int_{x>0}^{D_m} \frac{e^{-\frac{(\ln x - \mu_{cyc})^2}{2\sigma_{cyc}^2}}}{x\sigma_{cyc}\sqrt{2\pi}} dx$$
 (Eq. 15)

where $\mu_{cyc}=ln(D_{50})$ and $\sigma_{cyc}=ln[(D_{16}/D_{84})^{0.5}]$. Most computer spreadsheet applications have the cumulative lognormal distribution built into the function library. In 8.1 there is an example that illustrates how to determine the cyclone separator penetration function from the cumulative lognormal distribution given the cyclone separator's sharpness and D_{50} values.

NOTE: For most aircraft gas turbine engine applications all of the particulates will be <300 nm. In this size range the cyclone separator penetration function will be effectively equal to 1.0.

4.11.2 VPR Penetration Function, nvpr(Dm)

Particle losses in the VPR are due to both diffusion and thermophoresis. Since the penetration functions are multiplicative, the VPR penetration function will be the product of thermophoretic (e.g., 4.4) and diffusional penetration functions, i.e.,

$$\eta_{VPR} = \eta_{VPRth} \times \eta_{VPRdiff}$$
(Eq. 16)

This VPR penetration function is determined by fitting the theromophoretic and diffusional product to the VPR penetration values specified in AIR6241 [Reference 2.1.1.1]. The minimum values for these penetration fractions are given in Table 5. Note in this VPR penetration function, the thermophoretic factor, η_{VPRth}, is a constant parameter since the VPR and internal sample gas temperatures are held constant.

Table 5 - AIR6241 [Reference 2.1437] minimum specifications for VPR penetration at four particle diameters.

Particle Diameter,	Donatration Fraction
D _m (nm)	Penetration Fraction, η _{VPR}
15	≥0.3
30	≥0.55
50	≥0.65
100	≥0.70
	D _m (nm) 15 30

The diffusion factor, $\eta_{VPRdiff}$, is determined from standard particle losses due to diffusion in a laminar flow (e.g., Appendix A and [Reference 2.1.3.21]). Hence the total VPR penetration function is

$$\eta_{VPR} = \eta_{VPRth} \times \begin{cases} 1 - 5.5 \times \psi^{\frac{2}{3}} + 3.77 \times \psi & \psi < 0.007 \\ 0.819 \cdot e^{-11.5\psi} + 0.0975 \cdot e^{-70.1\psi} + 0.0325 \cdot e^{-179\psi} & \psi > 0.007 \end{cases}$$
(Eq. 17)

where the deposition parameter, $\psi = D X L_{VPR}/Q_{VPR}$, L_{VPR} is the effective length of the VPR, Q_{VPR} is the carrier gas flow in the VPR, and D is the particle diffusion coefficient calculated with the VPR temperature, T_{VPR} ,

$$D = \frac{k_B T_{VPR} C_c}{3\pi \mu D_m}$$

where C_c is the Cunningham slip correction factor and μ is the carrier gas viscosity. A more detailed discussion of this expression is given in 8.2, example 2 and in Appendix A. This equation along with the actual VPR particle penetration data (see Table 2) can be used to determine the VPR penetration function for a specific VPR. The equation can be fit to the four penetration points required in the AIR6241 [Reference 2.1.1.1] by varying the VPR effective length, L_{VPR} , and the value of the thermophoretic penetration constant, η_{VPRth} . The fit should be calculated by minimizing δ_{VPR} , the relative sum of squares difference between the measured VPR penetration, $\eta_{VPRmeas}$, and the calculated penetration function,

$$\delta_{VPR} = \sqrt{\sum_{D_m} \left(\frac{\eta_{VPRmeas}(D_m) - \eta_{VPR}(D_m)}{\eta_{VPRmeas}(D_m)}\right)^2}$$
 (Eq. 18)

The value of δ_{VPR} should be less than 0.05 to ensure a good fit to the measured penetrations.

Penetration fractions at 80 discrete particle sizes (D_m) in the range from 3 to 1000 nm should be calculated from the VPR continuous function.

4.11.3 CPC Counting Efficiency, nope

The AIR6241 [Reference 2.1.1.1] requires the CPC (as minimum requirements) to have counting efficiencies of ≥50% at an electrical mobility diameter of 10 nm and ≥90% at an electrical mobility diameter of 15 nm. Using the actual two CPC counting efficiencies with a two parameter sigmoid function [Reference 2.1.3.31] a continuous function for the CPC counting efficiency can be determined, i.e.,

$$\eta_{CPC} = 1 - e^{-\ln(2) \cdot \left[\frac{D_m - D_0}{D_{50} - D_0} \right]}$$
 (Eq. 19)

Using the two counting efficiency points the two parameters of the counting efficiency function can be determined analytically. The relationships between the function parameters and the counting efficiency points are

$$D_0 = \frac{\alpha_{10}D_{15} - \alpha_{15}D_{10}}{\alpha_{10} - \alpha_{15}}$$
 (Eq. 20)

$$D_{50} = \frac{(\alpha_{15}+1)D_{10}-(\alpha_{10}+1)D_{15}}{\alpha_{15}-\alpha_{10}}$$
 (Eq. 21)

where

$$\alpha_i = \frac{\ln(1 - \eta_{CPC,i})}{\ln(2)}, i = 10 \text{ or } 15$$
 (Eq. 22)

 D_{10} =10 nm, D_{15} =15 nm, $\eta_{CPC,10}$ is the counting efficiency at 10 nm and $\eta_{CPC,15}$ is the counting efficiency at 15 nm. In 8.3 an example of how to determine a CPC counting efficiency function from the above equations and the CPC counting efficiency specifications is given.

5. SIZE DISTRIBUTIONS AND SYSTEM LOSS CORRECTION FACTOR ESTIMATION

5.1 Size Distribution Assumptions

As discussed in the introduction, a lognormal size distribution is used to represent the engine exhaust plane non-volatile aerosol at the upstream end of the sampling system. The objective is to find a size distribution which has the same fractional nvPM mass concentration and number concentration losses as the exhaust aerosol. The size distribution at the engine exhaust nozzle exit plane, $\Delta nvPM_{numEP}(D_m)/\Delta ln(D_m)$, is specified by a total concentration $nvPM_{numEP}$, a geometric mean diameter, D_{mg} , and a geometric standard deviation, σ_g , explicitly,

$$\frac{\Delta nvPM_{numEP}(D_m)}{\Delta \ln(D_m)} = \frac{nvPM_{numEP}}{\sqrt{2\pi} \ln(\sigma_g)} \cdot e^{-\frac{1}{2} \left\{ \frac{\ln(D_m) - \ln(D_{mg})}{\ln(\sigma_g)} \right\}^2} = nvPM_{numEP} \cdot f_{lgn}(D_m)$$
 (Eq. 23)

Robust estimates of the size distribution parameter, σ_g , and the nvPM mass density, ρ , are available and based on engine test campaigns where size distributions were measured along with nvPM mass and number concentrations [References 2.1.3.1 through 2.1.3.13]. Most often, the size distributions were measured in the nvPM measurement Section (Section 5) of the sampling and measurement system (see Figure 4) near the nvPM mass and number instruments. Because of particle losses discussed above in the previous sections these downstream size distributions are reduced in nvPM mass and number concentrations and are distorted due to size dependent particle losses, especially for the smallest particle sizes which incur the highest losses. These losses are dependent on particle size, temperature, flow rate, and line geometry and can be represented by penetration and counting efficiency functions as discussed in Section 4. Figure 7 illustrates a comparison of size distributions at the nvPM number instrument (squares with dotted line), nvPM mass instrument (circles with dashed line), and the engine exhaust nozzle exit plane (triangles with solid line). Clearly, the size distributions at the nvPM mass and number instruments are reduced from the exhaust plane size distributions due to losses in the sampling and measurement system. The size distributions at the nvPM mass and number instruments differ due to the additional losses occurring in the VPR and the counting efficiency of the CPC.

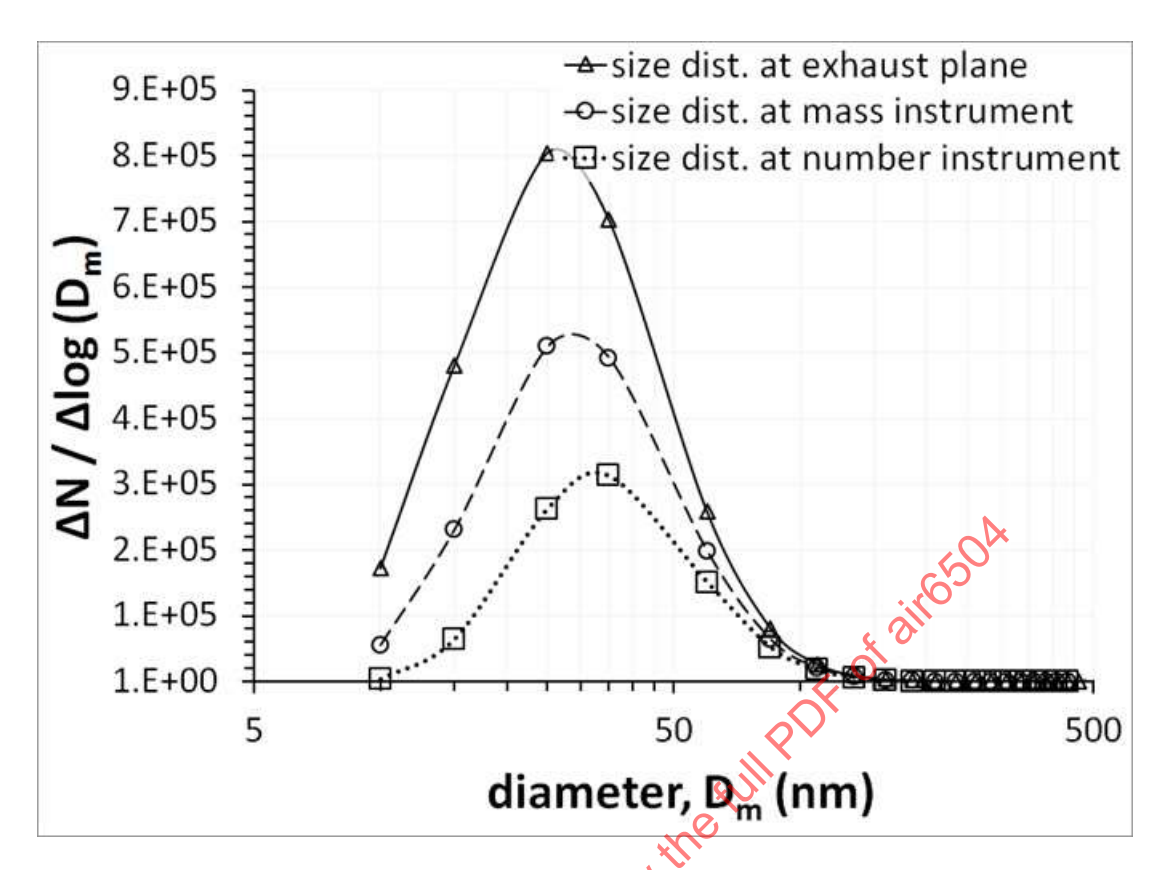


Figure 7 - Particle number size distributions at the engine exhaust plane, at the nvPM number, and at the nvPM mass instruments [Reference 2.1.3.1]

For this application the geometric standard deviation, σ_g =1.8, has been determined from research measurement campaigns [References 2.1.3.1 - 2.1.3.13]. The exhaust aerosol particles are represented by an equivalent sphere of a given diameter and have a corresponding effective nvPM mass density, ρ = 1 g/cm³. The effective density was determined using a differential mobility analyzer to determine the particle diameter and a centrifugal particle nvPM mass analyzer to determine the particle nvPM mass and then calculated as the ratio of the particle nvPM mass to the particle volume. Using the effective density accounts for the complex morphology of these particles. By using the nvPM mass to nvPM number concentration ratio, the only other parameter needed is the geometric mean diameter, D_{mg} , which is determined numerically in the loss calculation algorithm described in the next section.

5.2 Methodology for Estimating Engine Exhaust Plane Size Distributions

As described above, aircraft nvPM size distributions have been empirically determined to be lognormal. However, the AIR6241 [Reference 2.1.1.4] sampling and measurement system measures the nvPM mass and number concentrations after appreciable losses. The method to correct for these losses using nvPM mass and number measurements assumes that the engine exhaust plane lognormal nvPM size distribution is subjected to the calculated sampling and measurement system losses.

Estimated undiluted nvPM mass and number concentrations at the respective instruments can be calculated using the assumed lognormal size distribution at the exhaust nozzle exit plane, an assumed particle effective density, and the mass and number penetration fractions,

$$nvPM_{massEST} = \eta_{thermo} \times \sum_{D_m > 3nm}^{1000nm} \eta_{mass}(D_m) \times \frac{\rho \pi D_m^3}{6} \times nvPM_{numEP} \times f_{lgn}(D_m) \times \Delta \ln(D_m)$$
 (Eq. 23)

$$nvPM_{numEST} = \eta_{thermo} \times \sum_{D_m > 3nm}^{1000nm} \eta_{num}(D_m) \times nvPM_{numEP} \times f_{lgn}(D_m) \times \Delta \ln(D_m) \tag{Eq. 24}$$

Taking the mass to number ratio of these estimated values removes the unknown, nvPM_{numEP}, and leaves a single equation with a single unknown, i.e., the geometric mean diameter D_{mg} . Note, again, that the Probe inlet to Diluter1 inlet thermophoretic penetration factor, η_{thermo} , is separated from the other sampling system penetrations based on AIR6241 requirements [Reference 2.1.1.1].

To determine D_{mg} , this method repeatedly adjusts the geometric mean diameter, D_{mg} , of the exhaust nozzle exit plane nvPM number concentration size distribution, $f_{lgn}(D_m)$, while calculating the ratio, $R_{MN}(D_{mg})$, of the estimated nvPM mass to number concentrations with particle diameters ranging from 3 to 1000 nm,

$$R_{MN}(D_{mg}) = \frac{nvPM_{massEST}}{nvPM_{numEST}} = \frac{\eta_{thermo} \times \sum_{D_{m} > 3nm}^{1000nm} \eta_{mass}(D_{m}) \times \frac{\rho \pi D_{m}^{3}}{6} \times nvPM_{numEP} \times f_{lgn}(D_{m}) \times \Delta \ln(D_{m})}{\eta_{thermo} \times \sum_{D_{m} > 3nm}^{1000nm} \eta_{num}(D_{m}) \times nvPM_{numEP} \times f_{lgn}(D_{m}) \times \Delta \ln(D_{m})}$$

$$= \frac{\sum_{D_{m} > 3nm}^{1000nm} \eta_{mass}(D_{m}) \times \frac{\rho \pi D_{m}^{3}}{6} \times f_{lgn}(D_{m}) \times \Delta \ln(D_{m})}{\sum_{D_{m} > 3nm}^{1000nm} \eta_{num}(D_{m}) \times f_{lgn}(D_{m}) \times \Delta \ln(D_{m})}$$
(Eq. 25)

until the square of the relative difference, δ , between this ratio, $R_{MN}(D_{mg})$, and the ratio of the measured mass to number nvPM concentrations.

$$\frac{\eta_{thermo} \times DF_1 \times nvPM_{massSTP}}{\eta_{thermo} \times DF_1 \times DF_2 \times nvPM_{numSTP}}$$
 (Eq. 26)

is reduced to zero, i.e.,

$$\delta = \left[1 - \frac{\frac{R_{MN}(D_{mg})}{(\frac{\eta_{thermo} \times DF_1 \times nvPM_{musssTP}}{\eta_{thermo} \times DF_1 \times DF_2 \times nvPM_{numSTP}}}\right]^2 \cong 0$$
 (Eq. 27)

This method typically converges with values of δ <10⁻⁹. Note that the geometric standard deviation, σ_g , and the density, ρ , of the unknown aerosol are held constant with assumed values

$$\sigma_g = 18$$
 and $\rho = 1g/cm^2$.

The approach is summarized in Figure 3. Figure 7 illustrates typical size distributions with these constraints at the nvPM number instrument, nvPM mass instrument and at the engine exhaust nozzle exit plane.

5.3 nvPM Mass and Number Correction Factors

The ratio of upstream to downstream nvPM number concentrations gives a system loss correction factor for nvPM number and the ratio of upstream to downstream nvPM mass concentrations gives a system loss correction factor for nvPM mass. Note, however, that in determining the number and mass correction factors only particles with diameters of 10 nm or greater are used to calculate the number and mass correction factors. The number and mass correction factor equations are:

$$k_{SLnum} = \frac{\sum_{D_m>10nm}^{1000nm} nvPM_{numEP} \times f_{lgn}(\mathbf{D_m}) \times \Delta \ln(\mathbf{D_m})}{\sum_{D_m>3nm}^{1000nm} nvPM_{numEP} \times \eta_{num}(D_m) \times f_{lgn}(\mathbf{D_m}) \times \Delta \ln(D_m)}$$

$$=\frac{\sum_{D_{m}>1000nm}^{1000nm}\frac{1}{\sqrt{2\pi}\times\ln(\sigma_{g})}\times e^{-\frac{1}{2}\left\{\frac{\ln(D_{m})-\ln(D_{mg})}{\ln(\sigma_{g})}\right\}^{2}\times\Delta\ln(D_{m})}}{\sum_{D_{m}>3nm}^{1000nm}\frac{n_{num}(D_{m})}{\sqrt{2\pi}\times\ln(\sigma_{g})}\times e^{-\frac{1}{2}\left\{\frac{\ln(D_{m})-\ln(D_{mg})}{\ln(\sigma_{g})}\right\}^{2}\times\Delta\ln(D_{m})}}{\sum_{D_{m}>3nm}^{1000nm}\frac{n_{num}(D_{m})}{\sqrt{2\pi}\times\ln(\sigma_{g})}\times e^{-\frac{1}{2}\left\{\frac{\ln(D_{m})-\ln(D_{mg})}{\ln(\sigma_{g})}\right\}^{2}\times\Delta\ln(D_{m})}}{\sum_{D_{m}>3nm}^{1000nm}\eta_{num}(D_{m})\times e^{-\frac{1}{2}\left\{\frac{\ln(D_{m})-\ln(D_{mg})}{\ln(\sigma_{g})}\right\}^{2}\times\Delta\ln(D_{m})}}$$
(Eq. 28)

$$k_{SLmass} = \frac{\sum_{Dm>1000nm}^{1000nm} p_m^3 \times e^{-\frac{1}{2} \left\{ \frac{\ln(D_m) - \ln(D_{mg})}{\ln(\sigma_g)} \right\}^2 \times \Delta \ln(D_m)}}{\sum_{Dm>3nm}^{1000nm} \eta_{num}(D_m) \times D_m^3 \times e^{-\frac{1}{2} \left\{ \frac{\ln(D_m) - \ln(D_{mg})}{\ln(\sigma_g)} \right\}^2 \times \Delta \ln(D_m)}} \times \Delta \ln(D_m)$$
(Eq. 29)

From these corrections factors the final exhaust nozzle exit plane nvPM number and mass concentrations, nvPM_{numEP}(D_m>10 nm) and nvPM_{massEP} can be determined using

$$nvPM_{numEP} = k_{SLnum} \times k_{thermo} \times DF_1 \times DF_2 \times nvPM_{numSTP}$$
 (Eq. 30)

$$nvPM_{massEP} = k_{SLmass} \times k_{thermo} \times DF_1 \times nvPM_{massSTP}$$
 (Eq. 31)

Or the correction factors can be used to determine engine exhaust plane nvPM number and mass Emissions Indices using:

$$EI_{numEP} = k_{SLnum} \times EI_{num}$$
$$EI_{massEP} = k_{SLmass} \times EI_{mass}$$

since k_{thermo} is already included in the El calculation in AIR6241.

5.3.1 Calculation Tools

Based on the original UTRC spreadsheet tool [References 2.1.1.2, 2.1.3.12, 2.1.3.13, and 2.1.3.14] developed for the calculation of penetration fractions two additional tools, a spreadsheet based tool that uses Visual Basic to perform the calculations and a tool based in MATLAB® (requires a MATLAB® license to use source code), have been developed to perform the entire loss correction. They require the user to input the sampling and measurement system segment input parameters (see Table 2) and the mass and number concentrations.

These two tools are attachments to this AIR and have user manuals explaining how to use these tools. There is also a test dataset which can be used as an example of how to run these tools.

5.3.2 Loss Correction Excel® Spreadsheet

A spreadsheet based system loss calculation loss tool written in Microsoft® Excel® is available with this document. It allows calculation of system loss factors for a single data set or multiple data sets. It requires the user to input the sampling and measurement system segment input parameters (see Table 2) and the mass and number concentrations.

5.3.3 Loss Correction MATLAB® Tool

There is also available a loss correction calculator (both source code and an executable) based in MATLAB®. The user of the source code must have a MATLAB® license to run this version of the calculator. The executable version does not need a MATLAB® license. It too, of course, requires the user to input the sampling and measurement system segment input parameters (see Table 2) and the mass and number concentrations.

UNCERTAINTIES IN nVPM MASS AND NUMBER CORRECTION FACTORS

6.1 Parameter Uncertainties

An engine test campaign typically involves a number of runs at different conditions, e.g., power settings, different ambient conditions, fuel type, dilution levels, and engine type. At each test condition, typically lasting a few minutes, multiple measurements will be made for each measurement parameter. Each measurement parameter will have one or more systematic and random uncertainty contributions. These measurement parameter uncertainties will play three roles in the line loss correction model.

- 1. If size measurement data are taken, this data can be used in selecting adjustable parameters to make the line loss model give correction factors that agree with those computed on the basis of size measurements taken during engine test campaigns.
- 2. They will be used to estimate the uncertainty associated with the line loss model itself.
- 3. They will be used to estimate the total uncertainties in the nvPM mass and number correction factors once they are generated.

In the scope of this uncertainty analysis, two basic questions were posed:

- 1. What is the uncertainty in the correction factors?
- What drives the uncertainty in the correction factors?

To address the first question, a Monte Carlo analysis of the line loss correction was performed by assigning uncertainty to parameters in the line loss calculation. This generated a spread of correction factors to determine how uncertainty in the parameters drives uncertainty in the correction factors. To address the second question, an additional Monte Carlo analysis was done to determine the sensitivity of which parameter or parameters in the line loss correction drive the uncertainty when compared to the total uncertainty for the mass and number correction factors. For both of these Monte Carlo analyses a range of nvPM mass concentration (i.e., kthermoXDF1XnvPMmassSTP) and number concentration (i.e., kthermoXDF1XDF2XnvPMnumSTP) inputs were used to examine uncertainty in the nvPM mass and number correction factors as a function of particle size.

6.2 Overview of Monte Carlo Method

Typical nvPM number and mass correction factors are a function of particle diameter as shown in Figures 8 and 9. Nineteen different mass and number inputs were used to produce results for particle sizes over a representative range of engine exhaust particle sizes. To examine uncertainty of the number and mass correction factors for each of the particle sizes, a Monte Carlo simulation was performed to determine how the uncertainty in the parameters of the line loss calculation propagates to the uncertainty in the number and mass correction factors. The parameters that were assigned uncertainty were the measured inputs, the penetration functions and assumptions about the log-normal distribution. Each parameter uncertainty was assigned over a normally distributed range. Error estimates were given for the following model parameters and inputs:

- the measured nvPM mass
- 2. the measured number concentration
- 3. the mass segment line penetrations
- 4. the number segment line penetrations
- 5. the VPR penetrations at 15, 30, 50, and 100 nm
- 6. the CPC counting efficiency
- the log-normal distribution assumptions
 - a. the geometric standard deviation
 - the effective density

The error estimates used are listed in Table C1. There are other factors (see Document Scope and 7.1.3) not included in the model assumptions which are also not included in this analysis.

JULI POF OF air6504

Sources of systematic bias will have an impact on correction factor uncertainty determination, these biases are assumed to be small.

For a single Monte Carlo trial, error was randomly assigned to each parameter and the number and mass correction factors were calculated. This process was repeated 5000 times allowing for a population histogram to be constructed for both the number and mass correction factors. From the histograms, the total uncertainty for each correction factor was calculated as a spread of 67% of the population distribution. The analysis was done for each of the 19 points shown in Figures 8 and 9 to capture the spread of the number and mass correction factors as a function of particle size.

A detailed discussion on how the Monte Carlo method was implemented and how the uncertainty was assigned to each parameter can be found in detail in Appendix C.

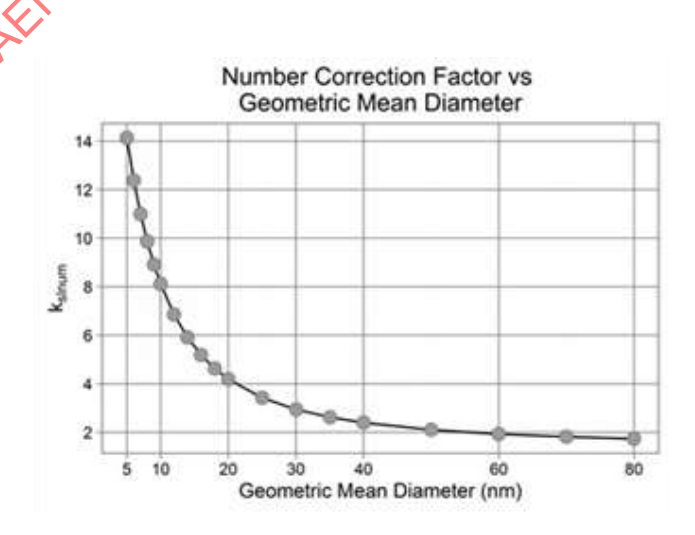


Figure 8 - Number correction factor versus exit plane geometric mean diameter

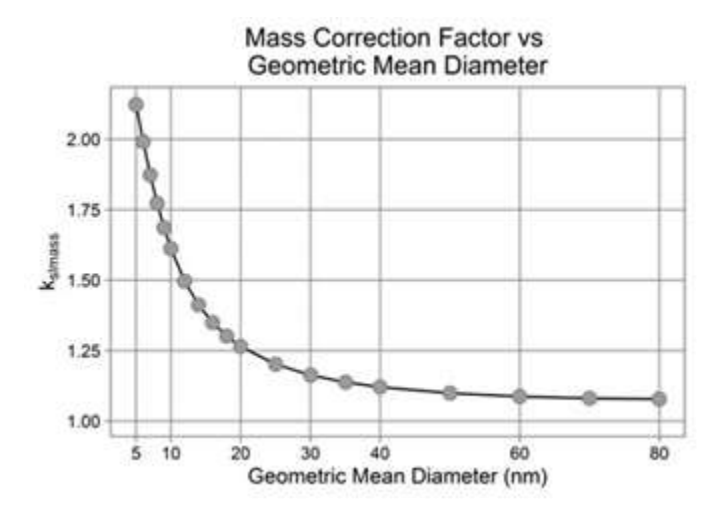


Figure 9 - Mass correction factor versus exit plane geometric mean diameter

To determine which parameter was driving the uncertainties in the full uncertainty analysis, a Monte Carlo sensitivity analysis was performed. For the sensitivity study, instead of applying uncertainty to all parameters of the line loss calculation, uncertainty was applied to only one parameter at a time and then a Monte Carlo calculation was done to determine the spread of correction factors. This calculation allowed for the comparison of the spread of the correction factors when only one uncertainty is applied in the line loss calculation to the full error propagation described above. This analysis was done for five different mass and number inputs for each model input parameter.

6.3 Results

6.3.1 Monte Carlo Uncertainty Propagation

The number and mass correction factors as a function of particle diameter shown in Figures 8 and 9 show that correction factors increase with decreasing geometric mean diameter. A Monte Carlo simulation was done for each of the 19 points shown in Figures 8 and 9 as the correction factors are a function of particle size. For each particle size, a population distribution was generated. The population distributions were then shifted and normalized by the population distribution median as shown in Equation 32.

$$\frac{\Delta k_{Slnum}}{k_{Slnum}} = \frac{k_{Slnum} \text{ at Nth percentile-} k_{Slnum} \text{ at 50th percentile}}{k_{Slnum} \text{ at 50th percentile}}$$
(Eq. 32)

The relative uncertainty distributions for 67% and 95% of the population distributions are plotted as a function of particle size in Figures 10 and 11. The relative number and mass uncertainty distribution spread increases with decreasing particle size. The number correction factor spread for 67% of the population for particles with a geometric mean size of 80 nm ranges between approximately -7% and +11% and at 5 nm the range is between approximately -25% and +36%. The mass correction factor spread for 67% of the population of particles with a geometric mean size of 80 nm ranges from approximately -0.5% to +0.4% and approximately from -10% to +13% for particles at 5 nm. A parametrization of the population spreads as a function of correction factor is located in Appendix C.

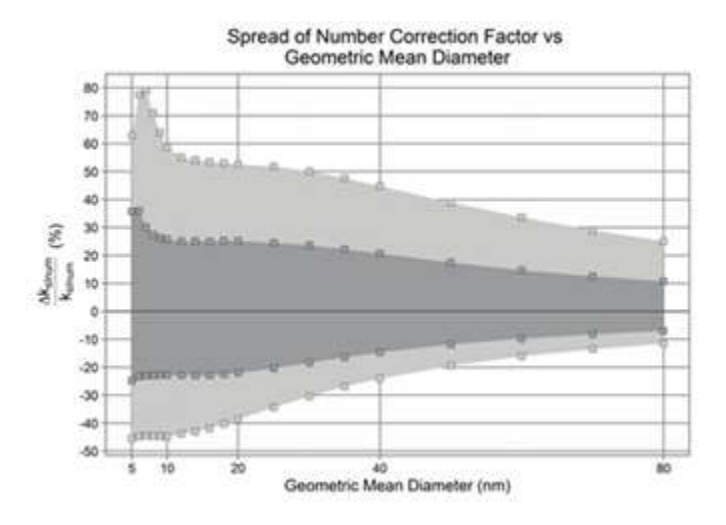


Figure 10 - Relative spread of number correction factor versus exit plane geometric mean diameter. The light grey and dark grey shaded areas indicate the 95% and 67% confidence intervals, respectively.

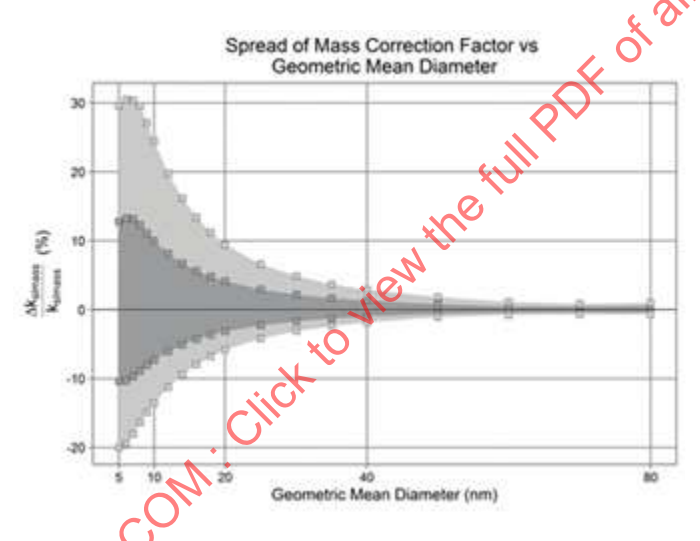


Figure 11 - Relative spread of mass correction factor versus exit plane geometric mean diameter. The light grey and dark grey shaded areas indicate the 95% and 67% confidence intervals, respectively.

6.3.2 Sensitivity Error Analysis Results

The population distributions for the sensitivity analysis were generated as described above. Each Monte Carlo simulation of 5000 trials consists of a single parameter allowed to vary at a number and mass setting that produces a particle size distribution with a geometric mean diameter. Each calculated population distribution is plotted as a box and whiskers plot where the top and bottom of the box represent the first and third quartiles of the distribution and the ends of the whiskers represent the 2.5% and 97.5% percentile of the distribution as shown in Figures 12 and 13.

Sensitivity simulations were done at geometric mean diameters of 5 nm, 10 nm, 20 nm, 40 nm, and 80 nm for the parameters shown in Figures 12 and 13. The results from the full error propagation analysis are included on the left side of each panel in the Figures for determination of what parameters generate the most uncertainty in the nvPM mass and number correction factors.

The sensitivity error analysis shows that the parameters that contribute the largest error in the calculation of the number correction factor, k_{SLnum}, are the geometric standard deviation, the measured mass, k_{thermo}XDF₁XnvPM_{massSTP}, and the measured number, k_{thermo}XDF₁XDF₂XnvPM_{numSTP}, as shown in Figure 12. For the mass correction factor the measured mass and the measured number contribute the most to error as illustrated by Figure 13.

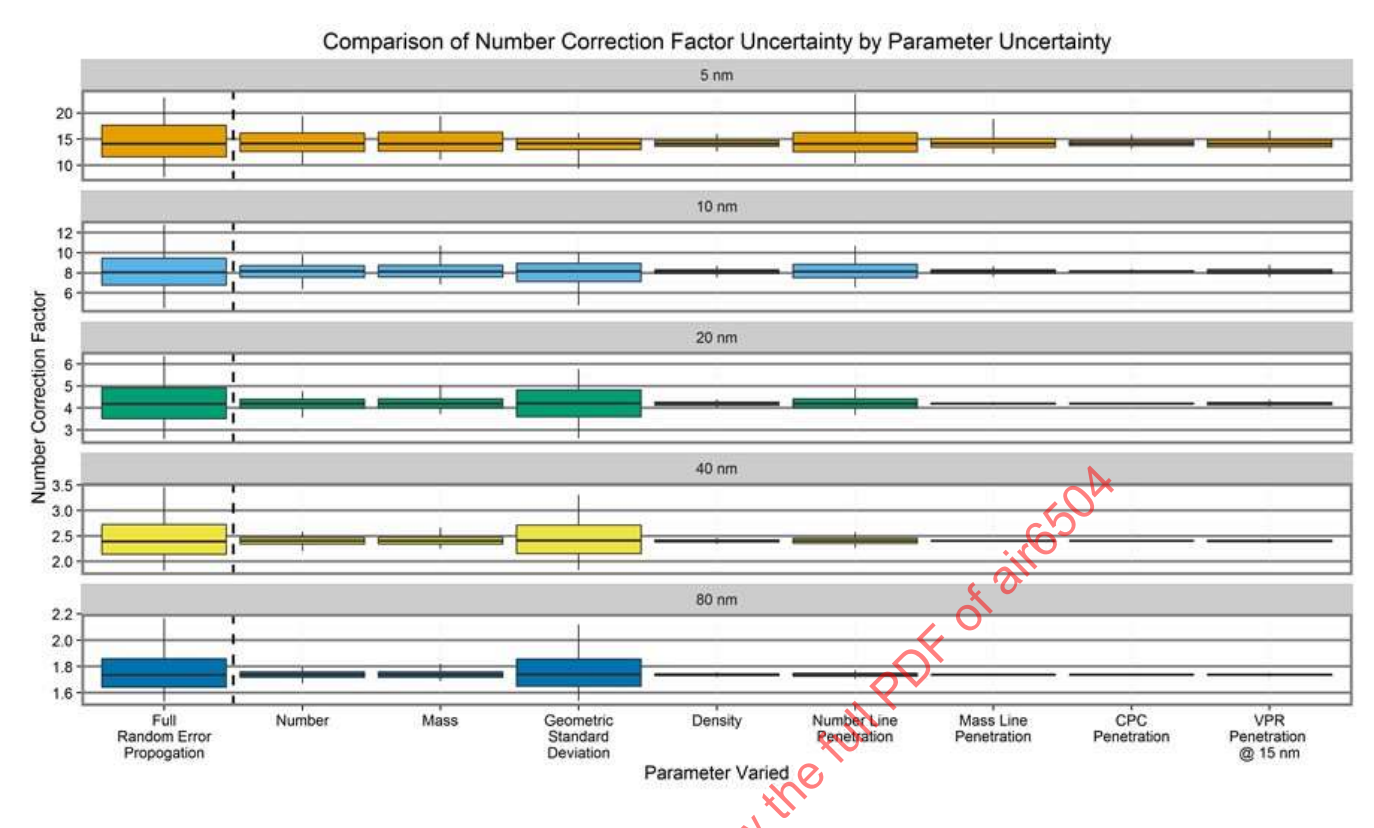


Figure 12 - Sensitivity analysis for the nvPM number correction factor. Note that the y-axis scale for each particle diameter is different.

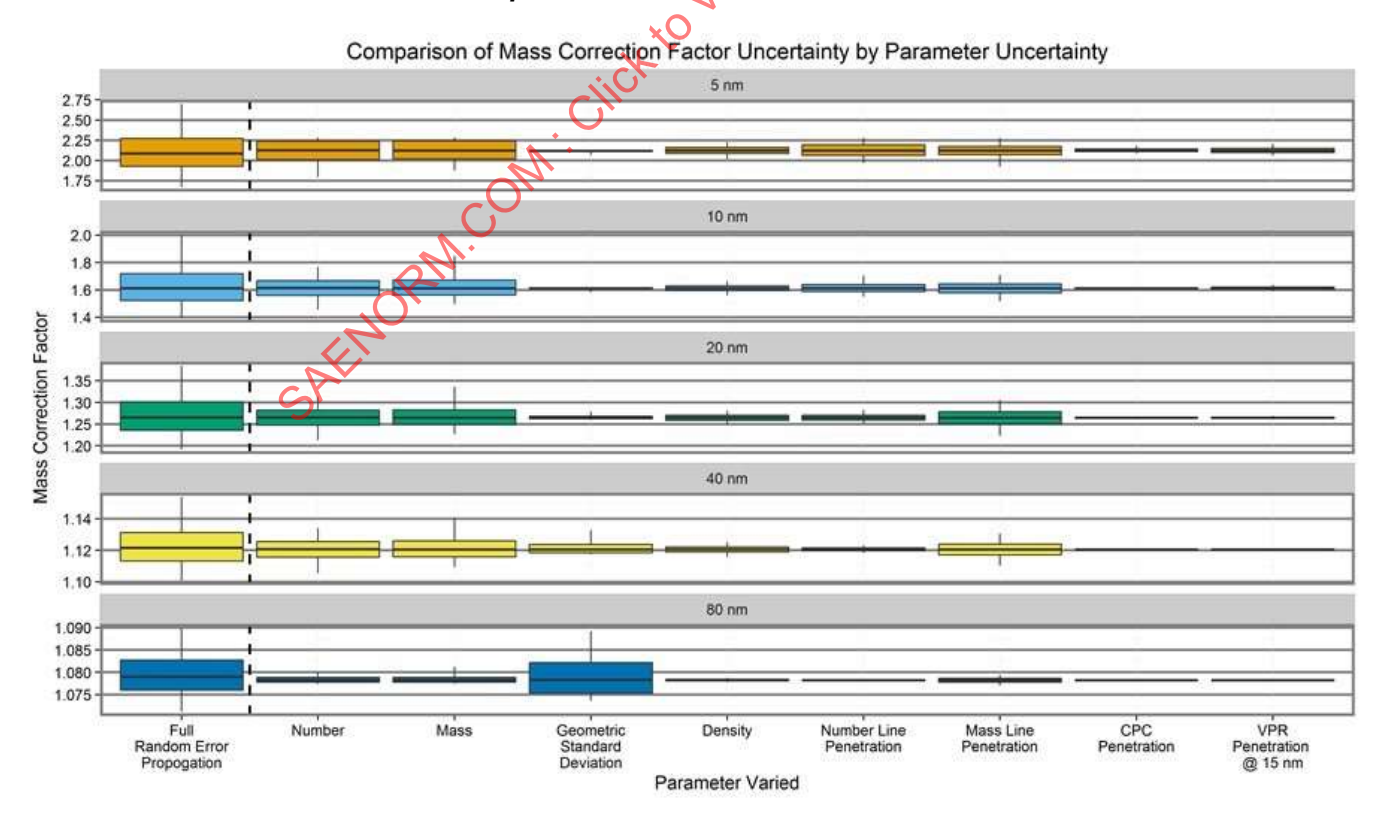


Figure 13 - Sensitivity analysis for the nvPM mass correction factor. Note that the y-axis scale at each diameter is different.

GENERAL INFORMATION ON METHOD ASSUMPTIONS AND ASSESSMENTS

7.1 Assumptions

The system loss correction factors are estimated based on the following assumptions: engine exhaust exit plane nvPM is represented by a constant value of nvPM effective density, a lognormal distribution, a fixed value of geometric standard deviation, no coagulation, limiting the nvPM mass concentration to the mass instrument limit of detection, and a minimum particle size cut-off of 10 nm.

7.1.1 Density

The current proposed value of effective density to be used in the model is determined from measured values (e.g., [Reference 2.1.3.7]). The model currently uses the value of 1 g/cm³. Line loss sensitivity calculations done using various values of density over the range of 0.55 to 1 g/cm³ show that line loss does not appear to have a strong dependence on effective density. There does appear to be a particle size dependence on effective density and the loss corrections [References 2.1.3.7 and 2.1.3.11]. As better data is available the model can accept improved values including a size dependent effective density to improve the accuracy of the model results.

7.1.2 Lognormal Distribution

Although aerosol size distributions are not universally characterized by any single function, those which have a continuous range of diameters on the order of a factor of 10 and nucleate and grow through diffusional collisions can typically be characterized by multi-modal lognormal size distributions. In this work a monomodal size distribution is used to represent the engine exhaust exit plane nvPM. The loss correction method's use of lognormal and monomodal size distributions has been checked with comparisons to measured size distributions and with sensitivity analyses using bimodal and trimodal size distributions. This analysis showed that line loss calculations using a single lognormal can give correction factors that are reasonably close to actual correction factors for multi-modal size distributions. However, there is still ongoing work to understand the method's sensitivity to the lognormal size distribution assumption.

7.1.3 Coagulation

This method does not consider reduction in particle nVPM number concentration due to coagulation. In the AIR6241 [Reference 2.1.1.1] sampling and measurement system Diluter1 is used to help reduce thermophoretic losses and to prevent particle coagulation. However, if the exit plane nVPM number concentration corrected for system losses and probe inlet to Diluter1 inlet thermophoretic losses is greater than 10⁸ particles/cm³, i.e., if

$$k_{SL_num} \times k_{inermo} \times DF_1 \times DF_2 \times nvPM_{numSTP} > 10^8 particles/cm^3$$
 (Eq. 33)

then particle coagulation may be occurring in the sampling system prior to Diluter1.

7.1.4 Penetration Drift

Line penetration drift has been evaluated for multiple systems. As of the date of this publication no significant drift has been observed over a period of about 10 months [Reference 2.1.3.32].

7.1.5 Correction Factors for Mass Measurements that are Below the Mass Instrument LOD

If the mass instrument measurement, nvPM_{massSTP}, is at or below the nvPM mass instrument LOD, M_{lod}, the correction factor can be determined by the following procedure.

First, D_{mgeff} (a geometric mean diameter to be used in the case when $nvPM_{massSTP} < M_{lod}$) can be determined from the arithmetic mean of maximum, D_{mgLOD} , and minimum, D_{mgMIN} , values of D_{mg} at the mass instrument LOD, i.e.,

$$D_{mgeff} = e^{\frac{1}{2}[\ln(D_{mgLOD}) + \ln(D_{mgMIN})]} = \sqrt{D_{mgLOD} \times D_{mgMIN}}$$
 (Eq. 34)

The maximum geometric mean diameter, D_{mgLOD} , is calculated using the procedure of Section 5 and Appendix B, from the dilution corrected measured value of nvPM number concentration, $DF_1XDF_2XnvPM_{numSTP}$ and the value of the mass instrument LOD as specified by the instrument manufacturer. (An example of this calculation is given in Example 8.4.) (Since the correction factors decrease with increasing particle diameter or geometric mean diameters, this maximum geometric mean value, D_{mgLOD} , represents a lower limit for the number concentration correction, k_{SLnum} .)

The geometric mean diameter lower limit, D_{mgMIN}, at the mass instrument LOD has been determined from test campaign data, D_{mgMIN}≈ 5 nm.

Since D_{mg} is the only parameter needed to determine the lognormal distributions, the value of D_{mgeff} from Equation 34 can be used along with the mass and number penetration functions to determine the mass and number correction factors and then the exit plane and measured nvPM mass and number concentrations. From Equations 35 and 36,

$$k_{SLmass} = \frac{\sum_{D_m > 10nm}^{1000nm} D_m^3 \times f_{lgn}(D_m) \times \Delta \ln(D_m)}{\sum_{D_m > 3nm}^{1000nm} \eta_{mass}(D_m) \times D_m^3 \times f_{lgn}(D_m) \times \Delta \ln(D_m)}$$
(Eq. 35)

$$k_{SLnum} = \frac{\sum_{Dm>1000m}^{1000nm} f_{lgn}(D_{m}) \times \Delta \ln(D_{m})}{\sum_{Dm>3m}^{1000m} \eta_{num}(D_{m}) \times f_{lgn}(D_{m}) \times \Delta \ln(D_{m})}$$
(Eq. 36)

The exit plane number is then computed from Equation 37,

$$nvPM_{numEP} = k_{SLnum} \times k_{thermo} \times DF_1 \times DF_2 \times nvPM_{numSTP}$$
 (Eq. 37)

and the exit plane mass is determined from the instrument OD value, nvPM_{massLOD}, i.e.,

$$nvPM_{massEP} = k_{stmass} \times k_{thermo} \times DF_1 \times nvPM_{massLOD}$$
 (Eq. 38)

The uncertainties in these values can be determined as explained in Section 6 describing the uncertainty analysis of this method.

Alternative methods that extrapolate D_{mo} or correction factors may also be applicable. For such extrapolations sufficient measurement data where $nvPM_{massLOD}$ must be available.

7.1.6 LOD for Number

CPC manufacturers report the CPC LOD to be about 1 particle/cm³. There is currently no alternative method to derive system loss correction factors when measured nvPM number concentrations are extremely low and close to the LOD.

7.1.7 Limits of Applicability

The correction factor calculator has been shown to work over a wide range of nvPM mass and number concentrations observed in aircraft turbine engine nvPM emissions. In cases where the calculator does not converge, the nvPM mass and number measurements are likely in error.

7.2 Collection Part Penetration Function, $\eta_1(D_m)x \eta_{b1}(D_m)$

Diagrams or verbal descriptions of in-use aircraft engine manufacturer nvPM sampling and measurement systems (Section 1 from probe tip to splitter1 inlet in Figure 4) were obtained from Pratt and Whitney, General Electric Aviation, Rolls Royce Civil Aerospace and Honeywell Aerospace and evaluated using the United Technologies Research Center (UTRC) particle transport model. Ignoring thermophoresis (which is a function of exhaust gas temperature and therefore independent of the sampling system Collection Part geometry), the primary loss mechanism during transport is particle diffusion. Diffusion losses increase as the sample tubing diameter decreases and as flow rate decreases. For the flow ranges and tube geometries of Section 1 of the nvPM sampling system, the tube diameters have a larger effect on diffusional losses than flow rate [Reference 2.1.3.33].

However, since a requirement for gas turbine emissions sampling multi-tip probes is that >80% of the pressure drop across the entire sample probe must be at the probe tips, extensive use of small diameter tubing is not practical. This design constraint forces the sampling system Collection Part used by all aircraft engine manufacturers to have relatively similar diffusional losses. For all aircraft engine manufacturer sampling and measurement systems a large proportion (~90% of the allowable 8 m) of the Section 1 sampling line has an inner diameter greater than 7 mm.

Similarly, although sample flow rate is a function of engine power, each aircraft engine manufacturer's Collection Part (Section 1), and in particular the sample probe, is designed and operated to acquire a limited range of flow rates which vary by a factor of 4 from low to high power. Typically, the lowest flow rate is 13.5 slpm to satisfy ARP1179 [Reference 2.1.1.5]. This variation in flow rate when sampling at low and high power conditions theoretically produces <5% difference in total particle loss. Therefore, the evaluated representative aircraft engine manufacturer configurations were found to have similar particle penetration curves from probe tip to the first splitter (i.e., the first 8 m of the emission sampling system corresponding to the Collection Part) with the typical penetration curve shown in Figure 14.

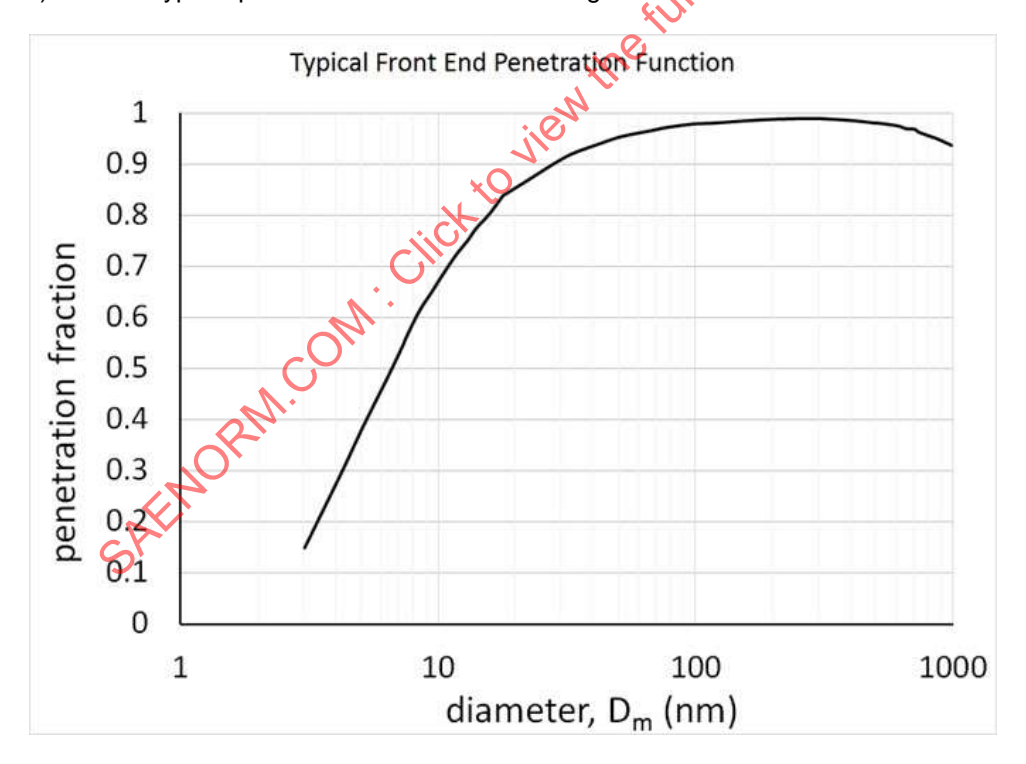


Figure 14 - Typical front end penetration curve, $\eta_1 x \eta_{b1}$, without thermophoresis losses determined from a comparison of four aircraft engine manufacturer representative Section 1 (from the sample probe tip to splitter1 inlet) particle emission sampling systems

7.3 Assessments

Since the publication of AIR6037 [Reference 2.1.1.2] additional experimental work [References 2.1.3.1 through 2.1.3.13] has been conducted to verify particle penetration calculations and the loss calculation methods presented in this work. Typically, what has been found is that the model is a robust method for calculating sampling and measurement system correction factors for particle losses. Errors in the method do increase with decreasing particle diameter which is due to the large particle losses at particle sizes below 10 nm. Additionally, in the effort to understand this calculation method, nvPM mass and number measurement errors can lead to unphysical loss calculation results. Hence, the tool can be used as a check on the sampling system measurements.

As an overview of the calculation method results, the two sub-paragraphs that follow give condensed data sets from test campaigns.

SAENORM. COM. Click to view the full PUTE of aircook

Table 6 - Correction factors determined from test campaigns

	APRIDE4					VARIANTI		
	(Nov. 2012) (DMS)	APRIDE5 (Aug. 2013) (DMS)	Honeywell (DMS, MSS)	Pratt& Whitney (DMS, MSS)	SAMPLE III.5 (April 2014)	(Sept. 2014) VARIANT II (Aug. 2015)	APRIDE8 (Nov 2015)	GE Aviation (2016)
k _{S∟num} Range: Ave. ± std. dev.:	2.0 to 3.6	2.3 to 6.0 4.15 ± 1.44	3.6 ± 0.8	4.6 ± 1.1	2.12 to 5.46	3.8 to 9.0 5.5 ± 1.3	2.2 to 7.3	1.77 to 18.6 4.86 ± 3.23
Error in k _{S∟num} : RMS or range	-27 to 2%	6 to 14%	7.9%	5.4%			<15% (when excluding Mass at LOD)	
k _{SLmass} Range : Ave. ± std. dev.:	1.2 to 1.4	1.06 to 1.19 1.12 ± 0.04	1.49 ± 0.09	1.3 ± 0.1	1.36 to 1.61	1.3 to 1.9 1.5 ± 0.2	7.18 to 1.7	1.11 to 3.02 1.49 ± 0.39
Error in k _{S∟mass} : RMS or range:	1.2 to 8%	5 to 13%	1.4	2.9%		>>//.	<12% (when excluding Mass at LOD)	
Num. of tests	9	39	21		8	90x2 28x2	9	42
Num. of engines	2	2	-	_	-	_	<u>~</u>	4
fuels			Cert. test fuel	Cert. test fuel	Jet	Jet A, Camelina, and blends	Jet A, and Jet A Solvesso blends	
Notes:	Applied a size dependent density. Note the range of corrections are within the range of the other campaigns. In general this does not affect the results.	Varied p and σ_a for parametric sensitivity analysis. See note for APRIDE4.		10/15. NOS.	Data stiffneeds further eds evaluation		Data still needs further evaluation	
validation	Errors in KSLnum and KSLmass determined from comparison of modelled values and values determined from size distribution measurements		Errors in kSLnum and kSLmass determined from comparison of modelled values and values defermined from size distribution measurements	and kSLmass omparison of nd values ize distribution		Analysis of two sampling and measurement system side by side comparisons; Careful and accurate size distribution measurements that allowed for validation of sampling system penetration fractions	Errors in kSLnum and kSLmass determined from comparison of modelled values and values determined from size distribution measurements	Errors in KSLnum and KSLmass determined from comparison of modelled values and values determined from size distribution measurements

7.3.1 VPR and 25 m Line Penetration Measurements

An illustration of data taken [Reference 2.1.3.11] to compare the UTRC line penetration calculation with actual measurement is illustrated in Figure 15.

From the same test campaign the VPR penetration function was also measured and compared with the model results. An example of the results is illustrated in Figure 16.

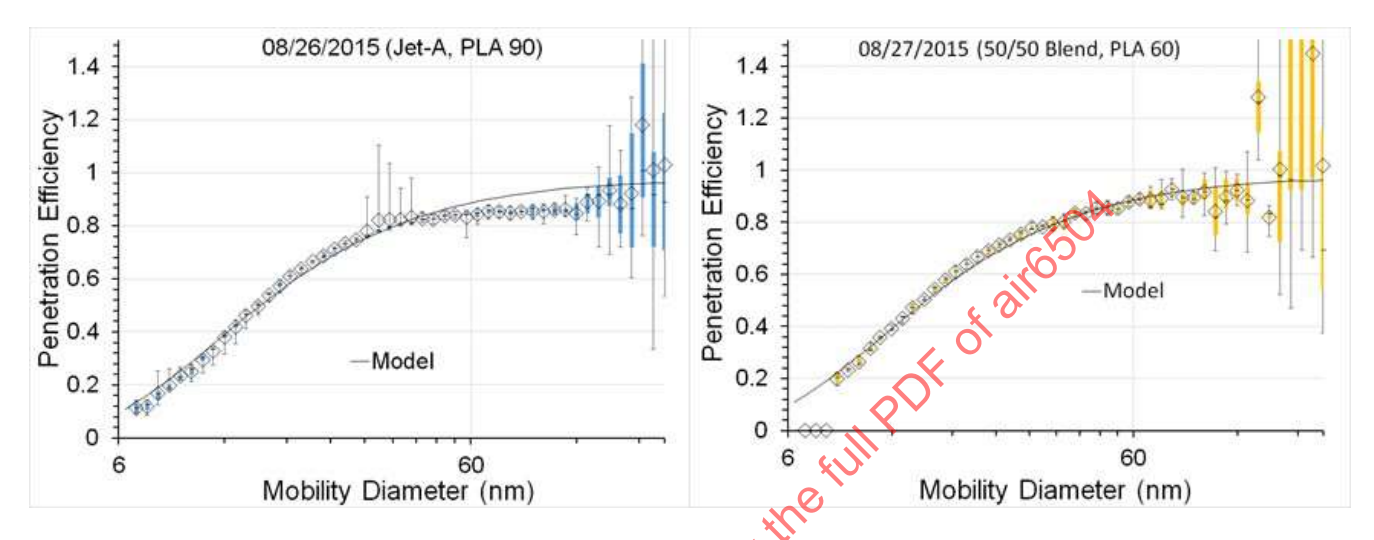


Figure 15 - Example of experimentally measured size dependent penetrations (diamonds with error bars) from two different days compared with the UTRC loss model (solid line). The data is a ratio of upstream to downstream size distributions measured with two SMPSs, one upstream and one downstream of the ARP 25 m line section. This measurement was taken at the aircraft turbine engine power level angle of 60. On 08/26/2015 the fuel was 100% Jet-A and on 08/27/2015 the fuel was a blend containing 50% Jet A and 50% Camelina. Note at large particle sizes where there are few particles counts at the tail of the size distribution the data shows a high degree of variability due to the low particle number statistics. Other test campaigns have reported similar results [e.g., References 2.1.3.3 through 2.1.3.6). The error bars represent the maximum and minimum penetration efficiency values for each diameter bin and the shaded areas represent the first and third quartiles for each diameter bin.

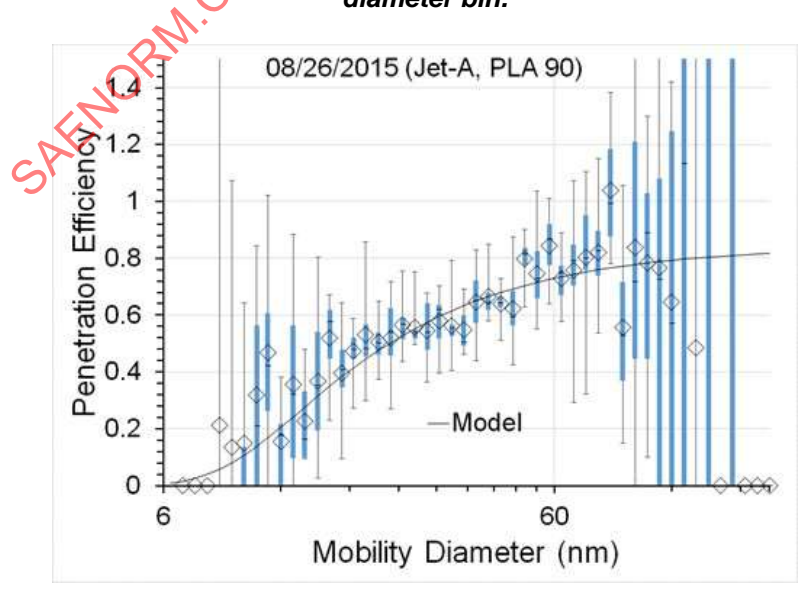


Figure 16 - Measured (diamonds with error bars) and modeled (solid line) VPR penetration efficiencies at high engine thrust. Signal was much noisier than line loss (Figure 15) due to low concentrations downstream of APC. VPR loss measurements were difficult to make in the field because of the high APC dilution ratio, i.e., DF2,

leading to low downstream concentrations. Although the results were noisy, the general trends agreed with manufacturer laboratory tests. The error bars represent the maximum and minimum penetration efficiency values for each diameter bin and the shaded areas represent the first and third quartiles for each diameter bin.

7.3.2 Expert Review of the System Loss Correction Method

During the preliminary work for setting the system loss correction method, the U.S. EPA sought in 2013 two independent experts on transport, sampling, and measurement of combustion engine exhaust PM emissions, Professors David Kittelson and K. Max Zhang of the University of Minnesota and Cornell University, respectively, to review the first draft of the method [References 2.1.3.18 and 2.1.3.34; also see Attachments I and II]. Essentially, they both have stated that:

- 1. The E-31 committee has spent a considerable amount of effort analyzing and developing methods for quantifying system losses for the measurement of non-volatile particulate matter emissions from aircraft engines, and
- 2. That the resulting overall methodology appears to be sound, although limited by the necessity of assuming engine exhaust nozzle exit plane geometric standard deviation and particle density.
- 3. Simulation calculations indicated that reasonable departures from assumed values geometric standard deviation density led to small errors in k_{SLmass}, typically less than 5%, but somewhat larger errors in k_{SLmass}, typically 20 to 25%.

They also provided ideas on how to potentially improve the proposed correction method and these have been integrated into the current methodology.

- 8. EXAMPLES OF SYSTEM LOSS CORRECTION METHODOLOGY
- 8.1 Example 1, Cyclone Separator Penetration Function

This explanatory information provides an example of calculating the cyclone separator penetration fraction function using example values for sharpness and D_{50} .

Given parameters:

$$D_{50} = 1000 \text{ nm}$$

Sharpness,
$$(D_{16}/D_{84})^{0.5} = 1.25$$

Step by step calculation:

1. Calculate µcyc

$$\mu_{\text{cyc}} = \ln(D_{50}) = \ln(1000 \text{ nm}) = 6.908$$

2. Calculate σ_{cyc}

$$\sigma_{\text{cvc}} = \ln[(D_{16}/D_{84})^{0.5}] = \ln(1.25) = 0.223$$

3. Input the values of μ_{cyc} and σ_{cyc} into the expression for the cyclone separator penetration fraction

$$\eta_{cyc}(D_m) = 1 - \int_{x>0}^{D_m} \frac{e^{\frac{-(\ln x - \mu_{cyc})^2}{2\sigma_{cyc}^2}}}{x\sigma_{cyc}\sqrt{2\pi}} dx = 1 - \int_{x>0}^{D_m} \frac{e^{\frac{-(\ln x - 6.908)^2}{2(0.223)^2}}}{x(0.223)\sqrt{2\pi}} dx$$

Below are values of $\eta_{cyc}(D_m)$, calculated using the above expression, for D_m values of 10, 100, and 1000 nm:

$$\eta_{cvc}(10 \text{ nm}) = 1$$

$$\eta_{cyc}(100 \text{ nm}) = 1$$

$$\eta_{cyc}(1000 \text{ nm}) = 0.50$$

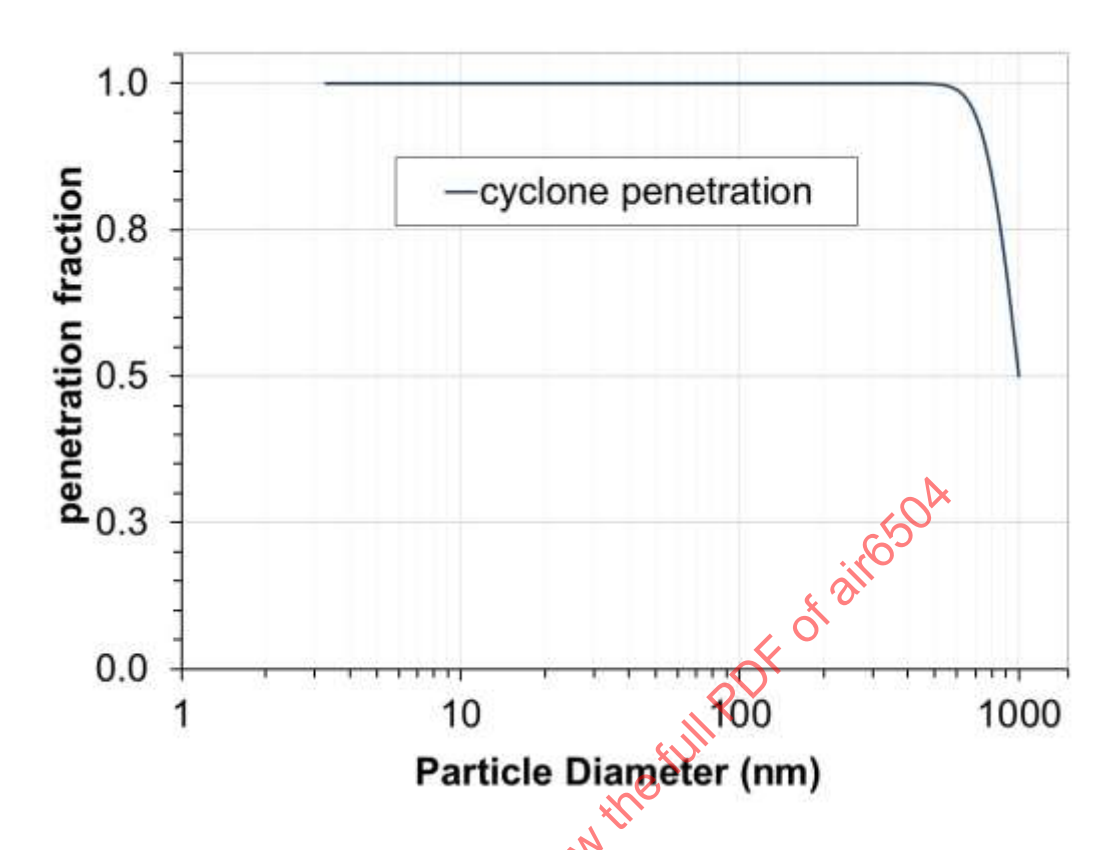


Figure 17 - Illustration of cyclone separator penetration function

8.2 Example 2, VPR Penetration Function

This explanatory information provides an example of calculating the VPR penetration function from particle thermophoretic loss and diffusional loss equations together with the four known and measured VPR penetration fraction specifications.

Given parameters and equations:

$$\eta_{VPR}(D_m=0.015 \mu m) = 0.314$$

$$\eta_{VPR}(D_m=0.030 \mu m) = 0.635$$

$$\eta_{VPR}(D_m=0.050 \ \mu m)=0.736$$

$$\eta_{VPR}(D_m=0.100 \ \mu m) = 0.778$$

T=350 °C, VPR temperature (350+273.15=623.15 K, the unit of temperature needed for these calculations is Kelvin). The VPR penetration function is given by the expression,

$$\eta_{VPR} = \eta_{VPRth} \times \begin{cases} 1 - 5.5 \times \psi^{\frac{2}{3}} + 3.77 \times \psi & \psi < 0.007 \\ 0.819 \cdot e^{-11.5\psi} + 0.0975 \cdot e^{-70.1\psi} + 0.0325 \cdot e^{-179\psi} & \psi > 0.007 \end{cases}$$

where,

 η_{VPRth} = parameter representing thermophoretic losses and is determined from the curve fitting step. The equation for ψ is

$$\psi = \frac{L_{VPR}}{Q_{VPR}} \times D = \frac{L_{VPR}}{Q_{VPR}} \times \frac{k_B T_{VPR} C_c}{3\pi \mu D_m} = \frac{k_B T_{VPR} C_c}{3\pi D_m \mu} \times \frac{L_{VPR}}{Q_{VPR}} \ .$$

where D_m= the particle diameter, L_{VPR} = the effective length of the VPR, C_c is the Cunningham slip correction factor, μ is the viscosity of air, and λ is the mean free path of air at the VPR temperature, T_{VPR}, and Q_{VPR} is the flow rate in the VPR. The ratio, L_{VPR}/Q_{VPR}, is used as a parameter of the curve fit to the manufacturer VPR penetration fractions. The expressions for the Cunningham slip correction factor, C_c, and the Sutherland equations for the gas mean free path, λ, and the viscosity, μ, are

$$C_c = 1 + \frac{2\lambda}{D_m} \left\{ 1.165 + 0.483 e^{-(0.997D_m/2\lambda)} \right\} = 1 + \frac{\lambda}{D_m} \left\{ 2.33 + 0.966 e^{-(0.4985D_m/\lambda)} \right\},$$

$$\lambda = \lambda_0 \left(\frac{T_{VPR}}{T_0} \right) \left(\frac{P_0}{P_{VPR}} \right) \left\{ \frac{1 + \frac{110.4}{T_0}}{1 + \frac{110.4}{T_{VPR}}} \right\}, \tag{Sutherland mean free path)}$$

and,

$$\mu = \mu_0 \left(\frac{T_{VPR}}{T_0}\right)^{3/2} \left(\frac{T_0 + 110.4}{T_{VPR} + 110.4}\right),$$
 (Sutherland viscosity)

respectively.

Step by step calculation:

Calculate the value for λ using the VPR temperature, T_{VPR}

$$\lambda = \lambda_0 \left(\frac{T_{VPR}}{T_0} \right) \left(\frac{P_0}{P_{VPR}} \right) \left(\frac{1 + \frac{S}{T_0}}{1 + \frac{S}{T_{VPR}}} \right)$$

aure, T_{VPR} , $\lambda = \lambda_0 \left(\frac{T_{VPR}}{T_0}\right) \left(\frac{P_0}{P_{VPR}}\right) \left(\frac{1+\frac{S}{T_0}}{1+\frac{S}{T_0}P_R}\right)$ nt, λ_0 =67.3 nm is 4P where S=110.4 K is the Sutherland constant, λ₀=67.3 nm is the reference mean free path at temperature T₀=296.15 K, and pressure P₀=P_{VPR}=101.325 kPa.

$$\lambda = 67.3nm \times \left(\frac{623.15}{296.15}\right) \times \left(\frac{101.325}{101.325}\right) \times \left(\frac{1+\frac{10.4}{296.15}}{1+\frac{110.4}{623.15}}\right) = 67.3nm \times 2.104 \times 1 \times \frac{1.373}{1.177} \cong 165nm$$

Calculate the value for μ using the VPR temperature, TVPR,

$$\mu = \mu_0 \left(\frac{T_{VPR}}{T_0}\right)^{3/2} \left(\frac{T_0 + 110.4}{T_{VPR} + 110.4}\right)$$

where =1.83 X 10^{-4} g/(cm s) is the reference viscosity at T_0 =296.15 K.

$$u = 1.83 \times 10^{-4} \frac{g}{cm \, s} \left(\frac{623.15}{296.15}\right)^{3/2} \left(\frac{296.15 + 110.4}{623.15 + 110.4}\right) = 3.10 \times 10^{-4} \frac{g}{cm \, s}$$

3. Calculate constants in the equation for ψ using the value of λ from above, i.e., the VPR temperature, T_{VPR}=623.15 K. The resulting equation is

$$\psi = \frac{k_B T_{VPR} L_{VPR}}{3\pi D_m Q_{VPR}} \times \frac{C_c}{\mu} = \frac{1.38065 \times 10^{-16} \frac{g \ cm^2}{s^2 \text{K}} \times 623.15 \text{K} \times \left[1 + \frac{165 nm}{D_m} \{2.33 + 0.966 e^{-(0.4985 D_m/165 nm)}\}\right]}{3\pi \times 3.10 \times 10^{-4} \frac{g}{cm \ s}} \times \frac{L_{VPR}}{D_m Q_{VPR}}$$

or

$$\psi = 2.945 \times 10^{-11} \, cm^3 / s \times \left\{ 1 + \frac{165 \, nm}{D_m} \left[2.33 + 0.966 e^{-\left(\frac{0.4985 \, D_m}{165 \, nm} \right)} \right] \right\} \times \frac{L_{VPR}}{D_m Q_{VPR}}.$$

Note : In the last term of this equation, L_{VPR}/D_mQ_{VPR} , D_m is in units of cm to make ψ unitless and in the other two occurances D_m is in units of nm.

4. Now, using this equation for ψ in the equation for η_{VPR} together with the four measured and known VPR penetrations fractions, i.e.,

$$\eta_{VPR}(D_m=15 \text{ nm}) = 0.314$$

$$\eta_{VPR}(D_m=30 \text{ nm}) = 0.635$$

$$\eta_{VPR}(D_m=50 \text{ nm}) = 0.736$$

$$\eta_{VPR}(D_m=100 \text{ nm}) = 0.778$$

a curve fitting routine can be used to determine the VPR penetration function. The parameters which will vary and will be determined by the curve fitting routine are the ratio of the effective length of the VPR to the flow in the VPR, L_{VPR}/Q_{VPR} , and the thermophoretic factor, η_{VPRth} .

For this example the VPR penetration function depicted in Figure 18 was determined. The curve fit parameters determined were $L_{VPR}/Q_{VPR}=98.2 \text{ s/cm}^2$ and $\eta_{VPRth}=0.877$. The calculated penetration fractions from the fit are

$$\eta_{VPR_{int}}(D_{m}=15 \text{ nm}) = 0.318$$

$$\eta_{VPR fit}(D_m=30 nm) = 0.609$$

$$\eta_{VPR}$$
 fit($D_m = 50 \text{ nm}$) = 0.729

$$\eta_{VPR_{it}}(D_{m}=100 \text{ nm}) = 0.813$$

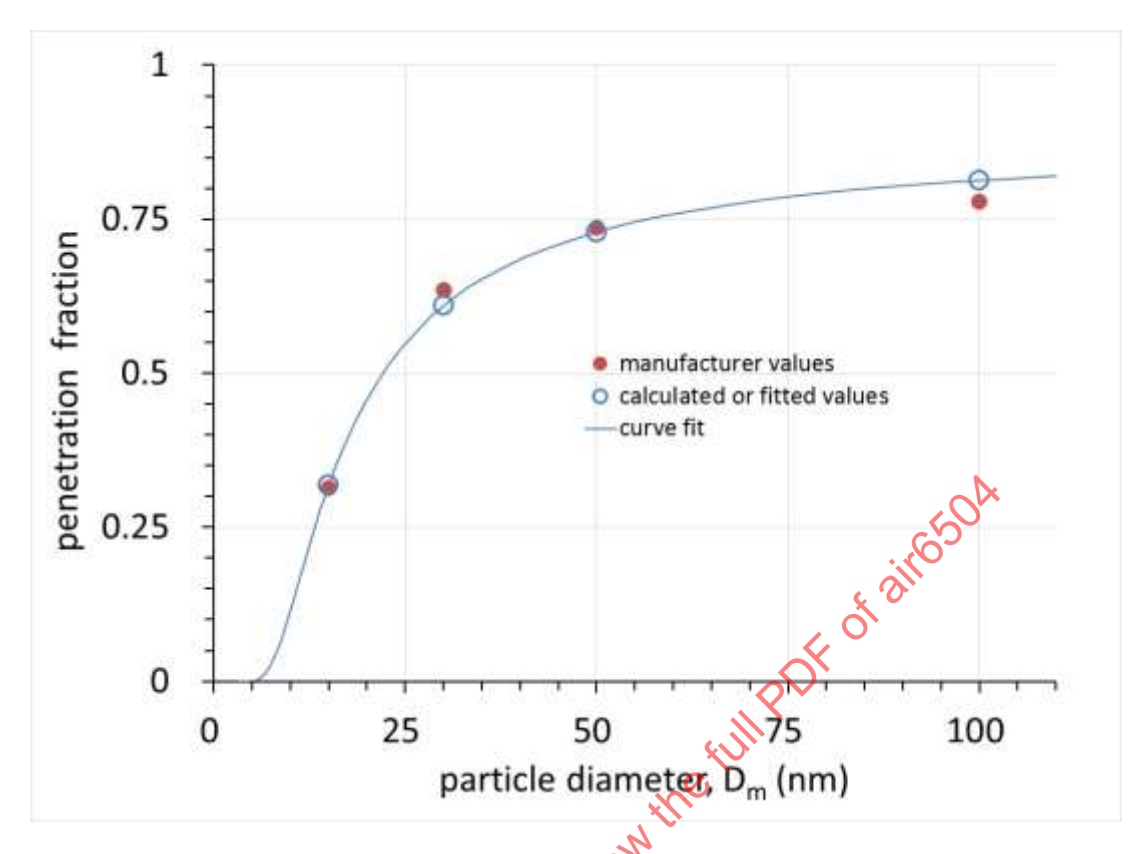


Figure 18 - Illustration of VPR penetration function

8.3 Example 3, CPC Counting Efficiency Function

This explanatory information provides an example of calculating the CPC counting efficiency function using the two CPC counting efficiencies specified for particles with diameters of 10 nm and 15 nm.

Given parameters:

 $D_{10} = 10 \text{ nm}$

 $D_{15} = 15 \text{ nm}$

 $\eta_{CPC,10} = 0.55$

 $\eta_{CPC,15} = 0.91$

Step by step calculation:

1. Calculate values for $\alpha_{10 \text{ nm}}$ and $\alpha_{50 \text{ nm}}$

$$\alpha_i = \frac{\ln(1 - \eta_{CPC,i})}{\ln(2)}, i = 10nm \text{ or } 15nm$$

$$\alpha_{10nm} = \frac{\ln(1 - 0.55)}{\ln(2)} = -1.152$$

$$\alpha_{15nm} = \frac{\ln(1 - 0.91)}{\ln(2)} = -3.474$$

Calculate D₀

$$D_0 = \frac{\alpha_{10}D_{15} - \alpha_{15}D_{10}}{\alpha_{10} - \alpha_{15}}$$

$$D_0 = \frac{(-1.152) * 15nm - (-3.474) * 10nm}{(-1.152) - (-3.474)} = 7.519nm$$

Calculate D₅₀

$$D_{50} = \frac{(\alpha_{15} + 1)D_{10} - (\alpha_{10} + 1)D_{15}}{\alpha_{15} - \alpha_{10}}$$

$$D_{50} = \frac{(-3.474 + 1) \times 10.0nm - (-1.152 + 1) \times 15nm}{(-3.474) - (-1.152)} = 9.673nm$$
Enter the calculated values into the expression for CPC counting efficiency

$$\eta_{CPC} = 1 - e^{-\ln(2) \cdot \left[\frac{D_m - D_0}{D_{50} - D_0} \right]}$$

$$\eta_{CPC} = 1 - e^{-\ln(2) \cdot \left[\frac{D_m - 7.519nm}{9.637nm - 7.519nm} \right]}$$

Below are values of $\eta_{CPC}(D_m)$, calculated using the above expression, for D_m values of 3.278 nm, 10.366 nm, and 50.481 nm: $\eta_{CPC}(3.278 \text{ nm}) = 0$ (If the value of the function is less than zero, then the value of the function should be set equal to zero.) $\eta_{CPC}(10.366 \text{ nm}) = 0.606$ $\eta_{CPC}(50.481 \text{ nm}) = 1.000$

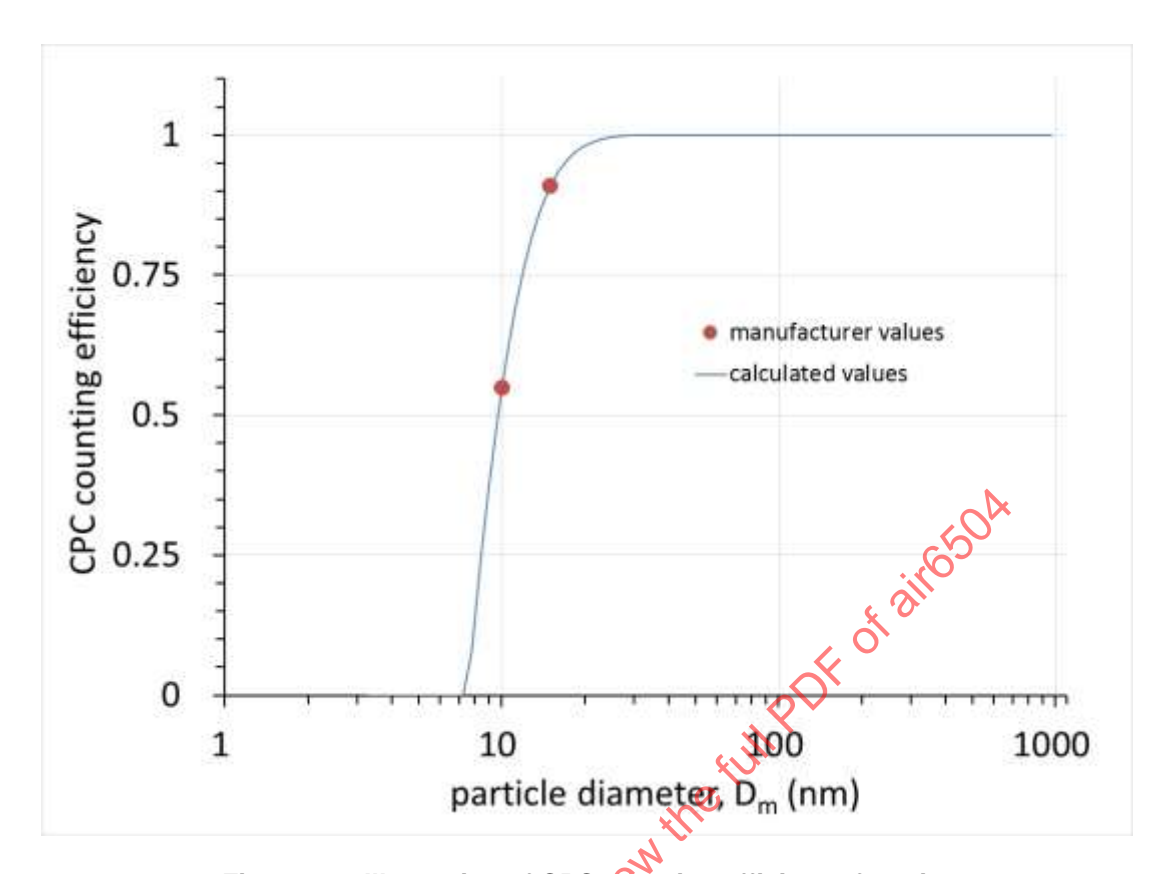


Figure 19 - Illustration of CPC counting efficiency function

8.4 Example 4, Example of Mass at LOD Calculation

Step by step calculation of the correction factors when the mass measurement is below the LOD of the mass instrument is given below.

1. Using the loss correction calculation tool calculate D_{mgMAX} from the measured number concentration, the instrument LOD, and the other needed system parameters

The nvPM number measurement, and dilution, DF1, and are as follows:

 $k_{thermo} = (750/433)^{0.38} = 1.232$

k_{thermo}XDF₂XnvPM_{STPn} (1.232)(4735.71 particles/cm³)=5834.39 particles/cm³

DF1=10

kthermoXDF2XDF1XnvPMsTPnum=58343.9 particles/cm³

For this example use the ARP6241 specified maximum instrument LOD, nvPM_{massLOD}=1 µg/m³

 $k_{thermo}XDF_1XnvPM_{massLOD} = 1.232X10X1 \mu g/m^3 = 12.32 \mu g/m^3$

Using the standard data inputs from the table above, the loss calculator yields

 $D_{mgLOD} = 35.13 \text{ nm}$

2. The geometric mean diameter can be calculated from the above value of D_{mgLOD} and the empirically determined minimum geometric mean value, D_{mgMIN}= 5 nm,

$$D_{mgeff} = \sqrt{D_{mgLOD} \times D_{mgMIN}} = \sqrt{35.13nm \times 5nm} = 13.25nm$$

3. Using the "Calcs" sheet in the calculation spreadsheet tool, the mass and number correction factors can simply be determined by entering D_{mgeff}=13.25 nm in cell Z20, see Figure 20. All other parameters are those from steps 1.) through 3.). The results are automatically calculated and displayed in cells AB4 (k_{SLmass}) and AB5 (k_{SLnum}),

ksLmass= 1.4933

 $k_{SLnum} = 5.4026$

SAEMORM. COM. Click to view the full PUTE of aircook

Table 7 - This example uses the loss tool and the standard input set listed in this table

			GANGED		PROBE	SPLITTER1 INLET TO		DILUTER1	25 M LINE TO CYCLONE SEPARATOR	SPLITTER2		SPLITTER2
NOTES:		INDIVIDUAL PROBE	PROBE ARM	GANGED PROBE	EXIT TO SPLITTER1	DILUTER1 INLET	DILUTER1 INLET	INLET TO 25 M LINE	AND SRLITTER2	TO APC DILUTER	APC DILUTER	TO NVPMMI
					SAMPLING	SAMPLING LINE INPUT PARAMETERS	4RAMETERS		×05			
SEGMENT ->		1	2	3	4	5	9	2	8	6	10	11
SEGMENT CARRIER GAS TEMPERATURE, Tarsu	¥	750	092	433	433	433	333	\$	333	333	333	333
SEGMENT PRESSURE, PO	кРа	101.33	101.33	101.33	101.33	101.33	101.33	101.33	101.33	101.33	101.33	101.33
SEGMENT FLOWRATE, Q ₁	mdls	4.17	12.50	12.50	50.00	2.50	7,250	25.00	25.00	4.50	4.50	3.45
SEGMENT TUBE DIAM, ID ₁	cm	0.150	0.435	0.775	0.775	0.775	0.099	0.775	0.775	0.400	0.400	0.400
SEGMENT LENGTH, L	cm	5.0	100.0	200.0	400.0	26.7	1.4	56.3	2499.4	170.2	15.9	134.6
SEGMENT LINE TEMPERATURE,	¥	750	092	433	433	EE#S.	333	333	333	333	333	303
SEGMENT BENDS, OBI	degrees	0	260	380	210	。 5,	0	0	1170	250	0	230
MASS/NUMBER FLAG	String	ВОТН	ВОТН	ВОТН	BQTH.	ВОТН	ВОТН	ВОТН	ВОТН	NUMB	NUMB	MASS
		000			W	ddy					3 0 0 0 0 0 0 0 0 0 0 0 0 0 0 0 0 0 0 0	
	n ₁₀ =	0.566			(mn) particle diam (nm)	liam (nm)	u			D ₅₀ (nm)	מומוכו	1000
	n ₁₅ =	0.917				15	0.312		Sharpı	Sharpness, (D ₁₆ /D ₈₄) ^{0.5}		1.221
				3		30	0.625					
				0		100	0.788					
				S								

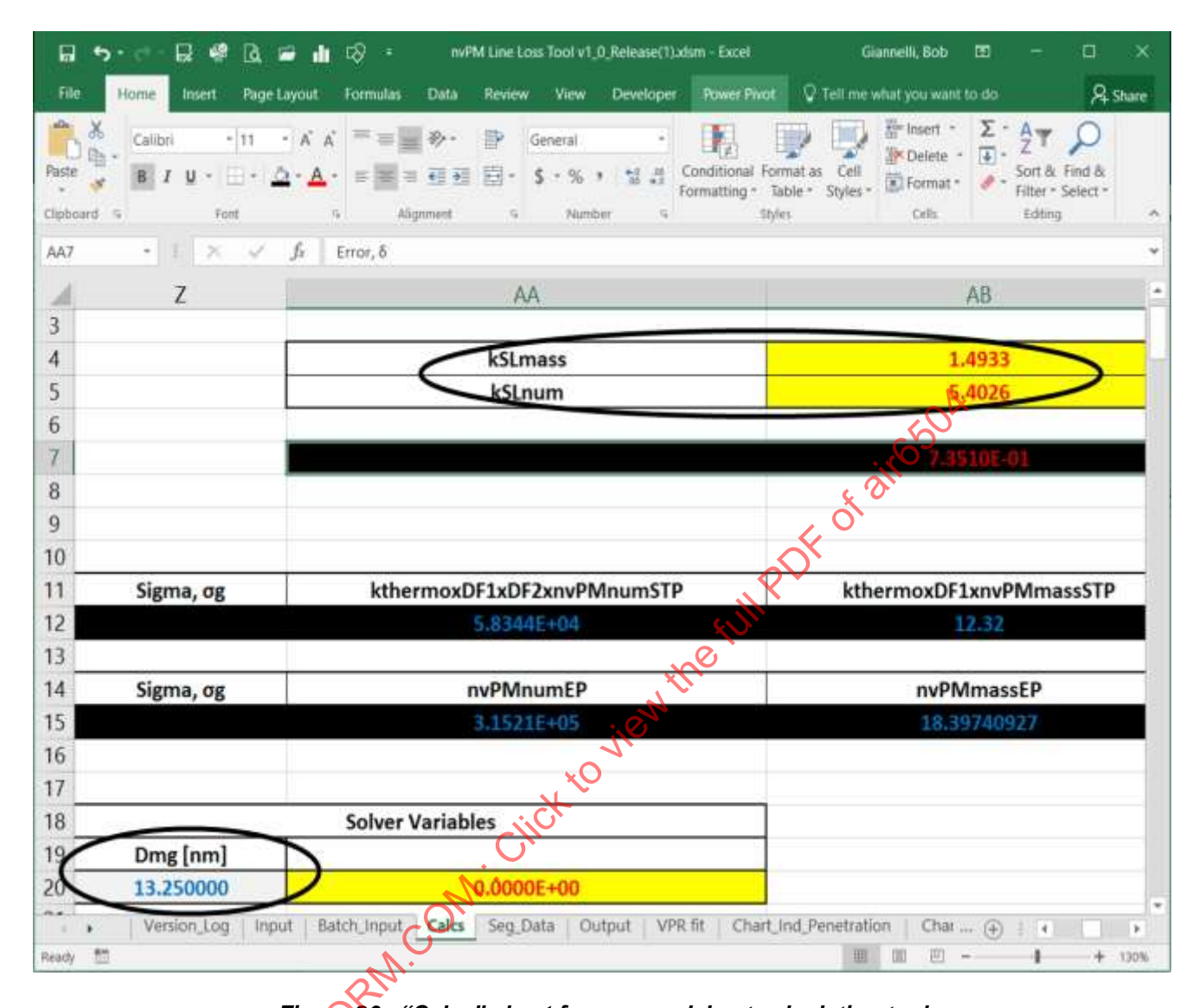


Figure 20 - "Calcs" sheet from spreadsheet calculation tool

9. NOTES

9.1 Revision Indicator

A change bar (I) located in the left margin is for the convenience of the user in locating areas where technical revisions, not editorial changes, have been made to the previous issue of this document. An (R) symbol to the left of the document title indicates a complete revision of the document, including technical revisions. Change bars and (R) are not used in original publications, nor in documents that contain editorial changes only.

APPENDIX A - PENETRATION FUNCTION DETAILS

A.1 THERMOPHORETIC PENETRATION FUNCTIONS

When the sample gas temperature at a segment inlet is higher than the segment sampling line temperature, the thermal gradient causes particles to move toward the cooler surface of the sampling line segment. This convective flow is in addition to the diffusional flow. Hence, thermal gradients ocurring because line temperatures are lower than gas temperatures cause additional particle deposition onto the sampling line surfaces. For particles with diameters that are less than the mean free path of the carrier gas, i.e., in the free molecular regime where the particles flow similar to the carrier gas, the particle thermophoretic deposition velocity is independent of particle diameter and pressure [References 2.1.3.3, 2.1.3.12, 2.1.3.13, 2.1.3.15].

The UTRC spreadsheet uses the thermophoretic expression [References 2.1.3.3, 2.1.3.12, 2.1.3.13, 2.1.3.14, and 2.1.3.15]

$$\eta_{thi} = \left[\frac{T_{linei}}{T_{gasi}}\right]^{Pr \times K_{th}} \cdot \left[1 + \left(\frac{T_{gasi}}{T_{linei}} - 1\right)e^{-\frac{\pi \times ID_i \times h_{gas} \times L_i}{\rho_{gas} \times Q_i \times C_p}}\right]^{Pr \times K_{th}}$$
(Eq. A1)

where T_{gasi} is the sample gas temperature in Kelvin, T_{linei} is the line wall temperature in Kelvin, ID_i is the line inner diameter, h_{gas} is the carrier gas convective heat transfer coefficient, L_i is the line length, ρ_{gas} is the carrier gas density, Q_i is the gas flow, C_p is the constant pressure carrier gas specific heat, P_i is the Prandtl number, and R_{th} is the thermophoretic coefficient,

$$K_{th} = \frac{2 \times C_s \times C_c}{1 + 3 \times C_m \times K_n} \left[2 + \frac{1}{\binom{k_g as}{k_n} + C_t \times K_n} \right]^{-1}$$
 (Eq. A2)

where C_s (= 1.17) is the slip coefficient, C_c is the Cunningham spectrum correction factor, C_m is the soot momentum, C_t is the thermal coefficient, k_{gas} is the thermal conductivity of the carrier gas, K_n (=2 λ /D_m) is the Knudsen number, λ is the carrier gas mean free path, and k_p is the particle thermal conductivity.

For a given sampling system set-up the gas and particle properties can be assumed approximately constant. Additionally, sampling lines are sufficiently long (>>10 cm) for the gas and particles to thermally equilibrate with the sampling line wall temperature. Thermophoretic losses will take place only when two connecting segments are at differing temperatures, Twallupstream and Twalldownstream, and the upstream segment is at a higher temperature than the segment directly downstream of it (Twallupstream>Twalldownstream) and connected to it. The thermophoretic loss will take place in the downstream segment whereby the inlet upstream gas temperature is equilibrated to the lower downstream segment wall temperature.

For the specific case of the thermophoretic loss from the Probe inlet to Diluter1 inlet in Sections 1 and 2, a simplified loss equation shall be used. It uses the segment wall temperature and the inlet gas temperature. In this simplified equation, the thermophoretic loss relationships have been shown [References 2.1.1.3 and 2.1.3.18] to reduce to

$$\eta_{thermo} \approx \left[\frac{T_{exit}}{Tin}\right]^{constant}$$
(Eq. A3)

where T_{in} is the temperature of the gas entering the sampling line which is approximately the engine exhaust temperature, i.e., $T_{in} \approx T_{EGT}$, T_{exit} is the equilibrated sample particulate and gas temperature which is approximately the temperature of the sampling line wall (i.e., the diluter inlet wall temperature, T_1), $T_{exit} \approx T_{wall} (=T_1)=433.15$ K, and the exponential constant is equal to 0.38. Hence, the thermophoretic penetration fractions for the segment 1 and 2 aircraft turbine engine work are assumed to follow

$$\eta_{thermo} = \left(\frac{T_1}{T_{EGT}}\right)^{0.38} \tag{Eq. A4}$$

where $T_1 = 433.15$ K or is the measured diluter inlet temperature, T_1 and T_{EGT} is the engine exhaust gas temperature (in Kelvin). Note that if $T_{EGT} \le T_1$, then $\eta_{thermo} = 1$.

If there are thermophoretic losses in other segments of the sampling and measurement system, the thermophoretic penetration fractions, η_{thi} , are determined from the UTRC thermophoretic expressions. These are explicitly shown above in Equations A1 and A2. For two adjoining segments the sample gas inlet temperature, T_{gasi} , is assumed to be the upstream

sample segment wall temperature, i.e., $T_{gasi} = T_{wallupstream}$. The wall temperature, $T_{linei} = T_{walldownstream}$, is the wall temperature of the downstream segment. There will be a thermophoretic correction needed, if the upstream segment wall temperature is greater than the downstream wall temperature, i.e., $T_{wallupstream} > T_{walldownstream}$.

A.1.1 Although, the simplified, Equation A4, and full thermophoretic loss calculations are sufficiently close and can be used interchangeably for this gas turbine engine application, the Excel spreadsheet and Matlab calculation tools supplied as part of this AIR use the full thermophoretic loss equation

A.2 DIFFUSIONAL LOSS PENETRATION FUNCTIONS

In the UTRC spreadsheet diffusional losses are modeled with standard models of particle diffusion in a turbulent flow [e.g., References 2.1.3.12, 2.1.3.13, 2.1.3.14, 2.1.3.15, 2.1.3.16, 2.1.3.20, and 2.1.3.21]. For diffusional losses the turbulent flow regime is used for all sampling system flows up to the instrument inlets even when the flow regime is laminar or transition. This will hold for all diffusional losses except the VPR. For the VPR laminar diffusion loss equations are used.

Penetration values, $\eta_i(D_m)$, for diffusional losses in these sampling system segments (excluding the VPR) are calculated with the expression

$$\eta_i(D_m) = e^{\frac{-\pi I D_i L_i V_{d,diff}}{Q_i}}$$
 (Eq. A5)

where $V_{d,diff}$ is the deposition speed, ID_i and L_i are the sampling line inner diameter and length, respectively, and Q_i is the gas flow in the sampling line. The expression for the deposition speed, $V_{d,diff}$ is

$$V_{d,diff} = 0.0118 \times Re^{\frac{7}{8}} \times Sc^{\frac{9}{3}} \times D/ID_i$$
 (Eq.

A6)

where Re is the Reynolds number,

$$Re = u_m \times \frac{\rho_{gas} \times ID_i}{\mu} = \left(\frac{4 \times Q_i}{\pi \times ID_i^2}\right) \times \frac{\rho_{gas} \times ID_i}{\mu} = \frac{4 \times Q_i \times \rho_{gas}}{\pi \times ID_i \times \mu}$$
 (Eq. A7)

Sc is the Schmidt number,

$$Sc = \frac{\mu}{\rho_{gas} \times D}$$
 (Eq. A8)

D is the diffusion coefficient,

$$D = \frac{k_B \times T_{gasi} \times C_c}{3 \times \pi \times \mu \times D_m}$$
 (Eq. A9)